

# A falling magnetic monopole as a holographic local quench

Nicolò Zenoni<sup>a,b,c</sup>, Roberto Auzzi<sup>a,b</sup>, Stefania Caggioli<sup>a</sup>,  
Maria Martinelli<sup>a</sup> and Giuseppe Nardelli<sup>a,d</sup>

<sup>a</sup> *Dipartimento di Matematica e Fisica, Università Cattolica del Sacro Cuore,  
Via Musei 41, 25121 Brescia, Italy*

<sup>b</sup> *INFN Sezione di Perugia, Via A. Pascoli, 06123 Perugia, Italy*

<sup>c</sup> *Instituut voor Theoretische Fysica, KU Leuven, Celestijnenlaan 200D, B-3001 Leuven, Belgium*

<sup>d</sup> *TIFPA - INFN, c/o Dipartimento di Fisica, Università di Trento,  
38123 Povo (TN), Italy*

E-mails: nicolo.zenoni@unicatt.it, roberto.auzzi@unicatt.it,  
stefy.caggioli@gmail.com, maria.martinelli1996@gmail.com,  
giuseppe.nardelli@unicatt.it

## Abstract

An analytic static monopole solution is found in global  $\text{AdS}_4$ , in the limit of small backreaction. This solution is mapped in Poincaré patch to a falling monopole configuration, which is dual to a local quench triggered by the injection of a condensate. Choosing boundary conditions which are dual to a time-independent Hamiltonian, we find the same functional form of the energy-momentum tensor as the one of a quench dual to a falling black hole. On the contrary, the details of the spread of entanglement entropy are very different from the falling black hole case, where the quench induces always a higher entropy compared to the vacuum, i.e.  $\Delta S > 0$ . In the propagation of entanglement entropy for the monopole quench, there is instead a competition between a negative contribution to  $\Delta S$  due to the scalar condensate and a positive one carried by the freely propagating quasiparticles generated by the energy injection.

# 1 Introduction

The AdS/CFT correspondence [1–3] provides a controlled environment to study the physics of a strongly-coupled conformal field theory (CFT) on the boundary by dealing with a weakly-coupled gravitational system in the Anti-de Sitter (AdS) bulk. In particular, it gives a very useful semiclassical picture of entanglement in strongly-coupled systems [4–6], by relating the entanglement entropy of a subsystem in a CFT to the area of an extremal surface anchored at the boundary of the subregion in the AdS dual. Holographic entanglement entropy is also important to understand black holes: for example, at finite temperature and in the limit of large subregions, the entanglement entropy is dominated by the thermodynamical contribution, and the Bekenstein-Hawking entropy [7, 8] is recovered.

The AdS/CFT correspondence provides several setups to investigate the thermalisation of out of equilibrium systems. Among these, quenches are conceptually simple theoretical settings, describing the evolution of a system triggered by a sudden injection of energy or a change of coupling constants. In the case of global quenches, the perturbation is spatially homogeneous and, in the bulk, it corresponds to the formation of a black hole. The evolution of the entanglement entropy has been studied in several examples of quench protocols, both on the CFT [9] and on the gravity side [5, 10–19]. While the simplest features of the spread of entanglement can be described by a model with free quasiparticles [9], a more detailed understanding needs to take into account the role of interactions [20].

A common feature of global quenches is that the energy is injected in the whole space. Once some perturbation in the entanglement entropy is detected, there is no clear way to discriminate the point where it originated. Local quenches allow for a more transparent analysis of the spread of quantum entanglement, because the initial perturbation is localised in a finite region of space. Moreover, local quenches can be realised in condensed matter systems such as cold atoms [21, 22] and they may provide a setup in which entanglement entropy might be measured experimentally [23, 24].

In CFT, local quenches can be modelled by joining two initially decoupled field theories [25, 26] and then evolving with a time-translation invariant Hamiltonian. Another approach in field theory is to consider excited states obtained by acting with local operators on the vacuum [27–30]. In holography, the latter kind of local quenches can be described by a free falling particle-like object in AdS [31]. The topic of local quenches was studied by many authors both on the CFT and on the gravity side: for example, mutual information was considered in [32] and finite temperature aspects were investigated in [33–35]. Bulk quantum corrections were recently studied in [36]. Local quenches obtained by splitting an initial CFT into two disconnected pieces were considered in [37].

In principle, the arbitrariness of choosing the falling particle on the gravity side corresponds to several choices of local quench protocols on the field theory side. In a local quench, it is interesting to understand which aspects of the physics are universal and which one depend on the details of the quenching protocol. This raises the question of how the choice of the falling particle in AdS affects the physics of the local quench of the boundary theory. Two natural candidates which are free of singularities are black holes (BH) or solitons. The black hole case was studied by several authors, see e.g. [31, 38, 39]. In this paper we will explore the possibility in which the falling particle is a soliton in  $\text{AdS}_4$ , focusing on the case of the ’t Hooft-Polyakov monopole [40].

Monopole solutions in global  $\text{AdS}_4$  have been considered by several authors, starting from [41, 42]. AdS monopole wall configurations have been studied in [43–46]. Holographic phase transitions for AdS monopoles have been investigated in [47–50]. In this paper, we will consider the theoretical setting introduced in [51]. In this situation, specialising to a multitrace deformation, the monopole in global AdS is dual to a theory with spontaneous symmetry breaking. A previous study of such a model was performed numerically. In

this work, we find an approximate analytic solution for the winding-one monopole, which includes the first-order backreaction on the metric.

Applying the change of variables introduced in [52], we map the time-independent global  $\text{AdS}_4$  solution to a falling monopole configuration in the Poincaré patch. On the field theory side, this is dual to a local quench in a perturbed CFT, induced by the injection of a condensate which breaks some of the global  $SU(2)$  symmetries of the theory. Outside the quench, the global symmetry of the CFT remains unbroken.

To investigate the field theory dual of the falling monopole, we compute the expectation values of various local operators. Depending on the choice of boundary conditions for the scalar, several interpretations are possible on the CFT side. For Dirichlet or Neumann boundary conditions, the falling monopole is dual to a CFT deformed by a time-dependent source, which performs a non-zero external work on the system. For a particular choice of the multitrace deformation, given in eq. (4.14), the monopole is dual to a theory with a time-independent Hamiltonian. In this case, the expectation value of the energy-momentum tensor has the same functional form as the one in the background of a falling black hole [31]. In other words, the energy density of the quench is not sensitive to the presence of the condensate.

To further characterise the field theory dual of the falling monopole, we perturbatively compute the entanglement entropy for spherical regions. Let us denote by  $\Delta S$  the difference of entropy between the excited state and the vacuum. We find a rather different behaviour for  $\Delta S$  compared to the case of the falling black hole: for the monopole quench,  $\Delta S$  for a region centered at the origin is always negative, while in the BH case  $\Delta S$  is positive. The negative sign of  $\Delta S$  for the monopole quench is consistent with the expectation that the formation of bound states, which are responsible for the condensate at the core of the quench, corresponds to a decrease of the number of degrees of freedom [53].

The paper is organised as follows. In section 2 we consider a static monopole solution in global AdS and we find an analytical solution in the regime of small backreaction. In section 3 we apply the change of variables introduced in [52] to the global AdS monopole. This trick transforms the global AdS static solution to a falling monopole in the Poincaré patch, which provides the holographic dual of the local quench. In section 4 we compute the expectation value of some local operators, including the energy-momentum tensor. In section 5 we study the entanglement entropy for various subsystem geometries. We conclude in section 6. Some technical details are discussed in appendices.

## 2 A static monopole in global AdS

We consider the same theoretical setting as in [51] which, in global AdS, is dual to a boundary theory with a spontaneously-broken  $SU(2)$  global symmetry. The action of the model is:

$$S = \int d^4x \sqrt{-g} \left[ \frac{1}{16\pi G} (R - 2\Lambda) + \mathcal{L}_M \right], \quad (2.1)$$

where  $\mathcal{L}_M$  is the matter lagrangian

$$\mathcal{L}_M = -\frac{1}{4} F_{\mu\nu}^a F^{a\mu\nu} - \frac{1}{2} D_\mu \phi^a D^\mu \phi^a - \frac{m_\phi^2}{2} (\phi^a \phi^a). \quad (2.2)$$

We choose the cosmological constant and the scalar mass as follows

$$\Lambda = -\frac{3}{L^2}, \quad m_\phi^2 = -\frac{2}{L^2}, \quad (2.3)$$

where  $L$  is the AdS radius. In eq. (2.2),  $F_{\mu\nu} = F_{\mu\nu}^a \frac{\sigma_a}{2}$  denotes the non-abelian field strength of the  $SU(2)$  gauge field  $A_\mu = A_\mu^a \frac{\sigma_a}{2}$ , i.e.

$$F_{\mu\nu}^a = \partial_\mu A_\nu^a - \partial_\nu A_\mu^a + e \epsilon^{abc} A_\mu^b A_\nu^c, \quad (2.4)$$

with  $e$  the Yang-Mills coupling. The covariant derivative acting on the adjoint scalar is

$$D_\mu \phi_a = \partial_\mu \phi_a + e \epsilon_{abc} A_\mu^b \phi^c. \quad (2.5)$$

The equations of motion are:

$$\begin{aligned} D^\mu F_{\mu\nu}^a - e \epsilon^{abc} \phi^b D_\nu \phi^c &= 0, & g^{\mu\nu} D_\mu D_\nu \phi^a - m_\phi^2 \phi^a &= 0, \\ R_{\mu\nu} - \frac{1}{2} R g_{\mu\nu} + \Lambda g_{\mu\nu} &= 8\pi G T_{\mu\nu}, \end{aligned} \quad (2.6)$$

where  $D_\mu$  denotes the combination of the gravitational and  $SU(2)$  gauge covariant derivatives, and  $T_{\mu\nu}$  is the bulk energy-momentum tensor

$$T_{\mu\nu} = D_\mu \phi^a D_\nu \phi^a + F_{a\mu\alpha} F_{a\nu}^\alpha + g_{\mu\nu} \mathcal{L}_M. \quad (2.7)$$

We first consider the monopole in a global  $AdS_4$  background, with metric

$$ds^2 = L^2 \left( -(1+r^2)d\tau^2 + \frac{dr^2}{1+r^2} + r^2(d\theta^2 + \sin^2\theta d\varphi^2) \right). \quad (2.8)$$

At large  $r$  the field  $\phi^a$  has the following expansion

$$\phi^a = \alpha^a \frac{1}{r^{\Delta_1}} + \beta^a \frac{1}{r^{\Delta_2}} + \dots, \quad (2.9)$$

where  $\Delta_{1,2}$  are the dimensions of the sources and vacuum expectation values (VEV) of the global  $SU(2)$  triplet of operators  $\mathcal{O}^a$  which are dual to the scalar triplet  $\phi^a$ . For our choice of mass, see eq. (2.3), the dimensions are

$$\Delta_1 = 1, \quad \Delta_2 = 2 \quad (2.10)$$

and both the  $\alpha^a$  and the  $\beta^a$  modes are normalisable. For this reason, we can choose among different possible boundary interpretations of the source and VEV<sup>1</sup>:

- the Dirichlet quantisation, where  $\alpha^a$  corresponds to the source and  $\beta^a$  to the VEV

$$J_D^a = \alpha^a, \quad \langle \mathcal{O}_2^a \rangle = \beta^a. \quad (2.11)$$

- the Neumann quantisation, where  $-\beta^a$  corresponds to the source and  $\alpha^a$  to the VEV

$$J_N^a = -\beta^a, \quad \langle \mathcal{O}_1^a \rangle = \alpha^a. \quad (2.12)$$

- the multitrace deformation [54–58], where  $\langle \mathcal{O}_1^a \rangle = \alpha^a$  and the boundary dual is deformed by the action term

$$S_{\mathcal{F}} = \int d^3x \sqrt{-h} [J_{\mathcal{F}}^a \alpha^a + \mathcal{F}(\alpha^a)], \quad J_{\mathcal{F}}^a = -\beta^a - \frac{\partial \mathcal{F}}{\partial \alpha^a}, \quad (2.13)$$

where  $\mathcal{F}$  is an arbitrary function. Imposing  $J_{\mathcal{F}}^a = 0$ , in order to consider an isolated system, we find the boundary condition

$$\beta^a = -\frac{\partial \mathcal{F}}{\partial \alpha^a}. \quad (2.14)$$

If we use either Dirichlet or Neumann quantisation, there is no non-trivial monopole solution with zero boundary scalar sources. Multitrace deformations, instead, allow finding a monopole solution with a zero boundary source (which satisfies eq. (2.14) for an opportune  $\mathcal{F}$ ), thus in a situation compatible with spontaneous symmetry breaking.

---

<sup>1</sup>The subscript in the operator  $\mathcal{O}^a$  refers to its dimension.

## 2.1 Monopole solution in the probe limit

Let us first consider the zero backreaction limit  $G \rightarrow 0$ . The monopole solution can be built by a generalisation of 't Hooft-Polyakov ansatz in global AdS<sub>4</sub> (see e.g. [41, 42, 51]):

$$\phi^a = \frac{1}{L} H(r) n^a, \quad A_l^a = F(r) r \epsilon^{aik} n^k \partial_l n^i, \quad (2.15)$$

where  $x^l = (r, \theta, \varphi)$  and  $n^k$  is the unit vector on the sphere  $S^2$

$$n^k = (\sin \theta \cos \varphi, \sin \theta \sin \varphi, \cos \theta). \quad (2.16)$$

The resulting equations of motion are shown in appendix A.1. The regularity of the solution at small  $r$  requires that both  $H(r)$  and  $F(r)$  approach zero linearly in  $r$ . On the other hand, at  $r \rightarrow \infty$ , the choice of boundary conditions depends on the physics we want to describe on the boundary. Such a choice is determined in terms of the coefficients  $(\alpha_H, \beta_H, \alpha_F, \beta_F)$  specified in the expansion of the scalar and gauge fields nearby the boundary:

$$H(r) = \frac{\alpha_H}{r} + \frac{\beta_H}{r^2} + \dots, \quad F(r) = \frac{\alpha_F}{r} + \frac{\beta_F}{r^2} + \dots. \quad (2.17)$$

We choose  $\alpha_F = 0$  in order to describe a theory with spontaneous breaking of the  $SU(2)$  global symmetry, as in [51]. Instead, in order to get a background which is different from empty AdS, we have to look for solutions where  $\alpha_H$  and  $\beta_H$  are generically non-vanishing. Once that  $\alpha_H$  is fixed,  $\beta_H$  is determined by the requirement that the solution is smooth. In appendix B we compute the monopole magnetic flux, which is independent of the boundary conditions expressed in eq. (2.17).

An exact solution to eqs. (A.1) can be found at the leading order in  $\alpha_H$ :

$$\begin{aligned} H(r) &= \frac{\alpha_H}{r} \left[ 1 - \frac{\tan^{-1} r}{r} \right], \\ F(r) &= \frac{e \alpha_H^2}{16 r^3} \left[ \pi^2 r^2 - 4 (r^2 + 1) (\tan^{-1} r)^2 - (\pi^2 - 4) r \tan^{-1} r \right]. \end{aligned} \quad (2.18)$$

Such a solution entails the following coefficients

$$\beta_H = -\frac{\pi}{2} \alpha_H, \quad \beta_F = e \alpha_H^2 \frac{12\pi - \pi^3}{32}. \quad (2.19)$$

At higher order in  $\alpha_H$ , eqs. (A.1) can be solved numerically. To this purpose, it is convenient to use the compact variable  $\psi$  defined by

$$r = \tan \psi. \quad (2.20)$$

The equations of motion in the variable  $\psi$  can be found in appendix A.2. An example of numerical solution is shown in figure 1. A plot of  $(\alpha_H, \beta_H)$  for various numerical solutions is shown in figure 2.

## 2.2 Monopole backreaction

We now introduce the monopole backreaction, modelled by the metric

$$ds^2 = L^2 \left( -(1 + r^2) h(r) g(r) d\tau^2 + \frac{h(r)}{g(r)} \frac{dr^2}{1 + r^2} + r^2 (d\theta^2 + \sin^2 \theta d\varphi^2) \right). \quad (2.21)$$

In order to recover asymptotically global AdS, we impose the following boundary conditions at large  $r$

$$\lim_{r \rightarrow \infty} h = \lim_{r \rightarrow \infty} g = 1. \quad (2.22)$$

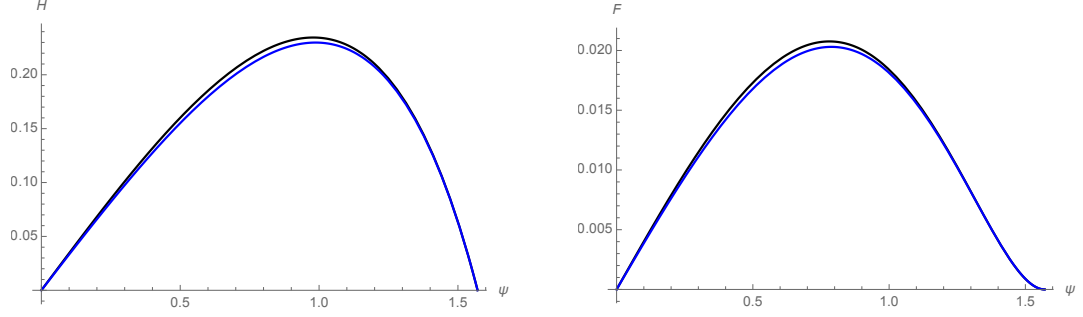


Figure 1: Numerical solutions for  $H(\psi)$  and  $F(\psi)$  are shown in black (the values  $e = 1$ ,  $\alpha_H = 1$  have been used). As a comparison, the analytical approximations (2.18) are shown in blue.

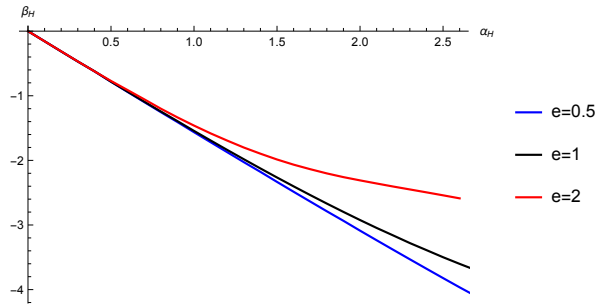


Figure 2: Plot of the relation between the coefficients  $\alpha_H$  and  $\beta_H$  for different values of  $e$ . At small  $\alpha_H$ , eq. (2.19) is satisfied.

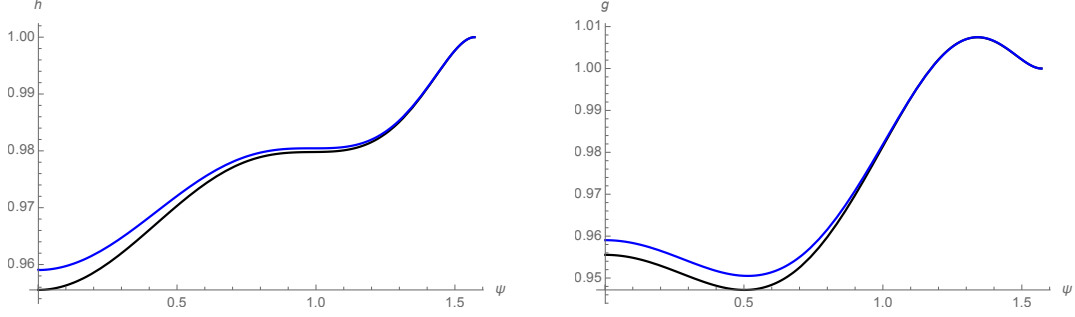


Figure 3: Numerical solutions for the metric functions  $h(\psi)$  and  $g(\psi)$  are shown in black (the values  $e = 1$ ,  $\alpha_H = 1$ ,  $L = 1$  and  $G = 0.1$  have been used). As a comparison, the analytical approximations (2.26) are shown in blue.

The full set of equations of motion in this background is given in appendix A.1.

The asymptotic form of the equations of motion fixes the following large  $r$  expansions

$$h(r) = 1 + \frac{h_2}{r^2} + \frac{h_3}{r^3} + O(1/r^4), \quad g(r) = 1 + \frac{g_2}{r^2} + \frac{g_3}{r^3} + O(1/r^4), \quad (2.23)$$

with

$$g_2 = -h_2 = \frac{2\pi G \alpha_H^2}{L^2}, \quad h_3 = -\frac{16\pi G}{3L^2} \alpha_H \beta_H. \quad (2.24)$$

The unfixed parameter  $g_3$  can be found by requiring that the solution is smooth.

At the leading order in  $\alpha_H$ , the  $H(r)$  and  $F(r)$  solutions are still given by eq. (2.18). The leading-order backreaction on the metric can be solved analytically too, giving:

$$h(r) = 1 + \epsilon h_\epsilon + O(\epsilon^2), \quad g(r) = 1 + \epsilon g_\epsilon + O(\epsilon^2), \quad \epsilon = \frac{\pi G \alpha_H^2}{L^2}, \quad (2.25)$$

where

$$\begin{aligned} h_\epsilon &= \pi^2 - \frac{4}{r^2} - \frac{2}{r^2 + 1} - 4 \frac{2(r^2 - 1)r \tan^{-1} r + (r^4 + 1)(\tan^{-1} r)^2}{r^4}, \\ g_\epsilon &= \pi^2 + \frac{1}{r^2} - \frac{2r \tan^{-1} r + 3}{r^2} \left(1 - \frac{2}{1 + r^2}\right) \\ &\quad - 2(\tan^{-1} r) \frac{2(r^4 - 1) \tan^{-1} r + r(3r^2 + 4)}{r^4}. \end{aligned} \quad (2.26)$$

These solutions set

$$g_3 = -\frac{10\pi^2 G \alpha_H^2}{3L^2}. \quad (2.27)$$

The profile functions at higher order in  $\alpha_H$  are again accessible by numerically solving the equations of motion. As in the probe limit, it is convenient to introduce the variable  $\psi = \tan^{-1} r$ , getting the equations of motion shown in appendix A.2. A comparison between the numerical and the analytical solutions at small  $\alpha_H$  is shown in figure 3.

### 3 A falling monopole in Poincaré patch

The gravity dual of local quench in a CFT can be realised by considering a falling particle in AdS [31]. To this purpose, a nice trick was introduced in [52]. The idea is to start from a spherically symmetric geometry in global AdS, and to transform it to a time-dependent Poincaré AdS geometry by performing a change of variables.

The Poincaré AdS<sub>4</sub> metric with coordinates  $(t, z, x, \varphi)$  is

$$ds^2 = L^2 \left( \frac{dz^2 - dt^2 + dx^2 + x^2 d\varphi^2}{z^2} \right). \quad (3.1)$$

The metric in eq. (3.1) and the global AdS metric in eq. (2.8) can be mapped into each other via the coordinate transformations

$$\begin{aligned} \sqrt{1+r^2} \cos \tau &= \frac{A^2 + z^2 + x^2 - t^2}{2A z}, & \sqrt{1+r^2} \sin \tau &= \frac{t}{z}, \\ r \sin \theta &= \frac{x}{z}, & r \cos \theta &= \frac{z^2 + x^2 - t^2 - A^2}{2A z}, \end{aligned} \quad (3.2)$$

leaving the angular coordinate  $\varphi$  unchanged.

These transformations can be inverted as follows:

$$\begin{aligned} r &= \frac{\sqrt{A^4 + 2A^2(t^2 + x^2 - z^2) + (z^2 + x^2 - t^2)^2}}{2A z}, \\ \tau &= \tan^{-1} \left( \frac{2A t}{z^2 + x^2 - t^2 + A^2} \right), \\ \theta &= \tan^{-1} \left( \frac{2A x}{z^2 + x^2 - t^2 - A^2} \right). \end{aligned} \quad (3.3)$$

The change of variables in eq. (3.2) maps a configuration with a static particle in the center of global AdS to a falling particle in the Poincaré patch, that can be used to model a local quench. We will apply this method to the monopole solution we discussed in section 2.

The holographic quench is symmetric under time reversal  $t \rightarrow -t$ : for  $t < 0$  the monopole is approaching the boundary, while for  $t > 0$  it moves in the direction of the bulk interior. Physically, we can think of the initial condition at  $t = 0$  as the initial out-of-equilibrium state, which can be prepared in the dual conformal field theory by some appropriate operator insertion.

The position of the monopole center, corresponding to  $r = 0$  in global AdS, in the Poincaré patch is time-dependent and follows the curve

$$x = 0, \quad z = \sqrt{t^2 + A^2}. \quad (3.4)$$

In the approximation in which the monopole is a pointlike particle, eq. (3.4) can be interpreted as the trajectory of the monopole. From the gravity side, the parameter  $A$  can be interpreted as the initial position along the  $z$ -direction of the free-falling monopole. From the CFT perspective, the parameter  $A$  fixes the size of the local quench.

### 3.1 Bulk energy density of the falling monopole

One may be tempted to imagine the monopole as a pointlike particle which is falling along the trajectory in eq. (3.4). To check this intuition, it is natural to consider the bulk energy-momentum tensor (2.7).

Working in the limit of negligible monopole backreaction, we perform the coordinate change in eq. (3.3)

$$x^\mu = (\tau, r, \theta, \varphi) \rightarrow x'^\mu = (t, z, x, \varphi) \quad (3.5)$$

The energy-momentum tensor in Poincaré patch is given by

$$T'_{\alpha\beta}(x') = \frac{\partial x^\mu}{\partial x'^\alpha} \frac{\partial x^\nu}{\partial x'^\beta} T_{\mu\nu}(x). \quad (3.6)$$



To properly normalise the energy-momentum tensor, we introduce the vierbein  $e_m^\mu$  such that

$$T'_{mn}(x') = e_m^\mu e_n^\nu T'_{\mu\nu}(x'), \quad e_m^\mu e_n^\nu g'_{\mu\nu} = \eta_{mn}, \quad (3.7)$$

where  $g'_{\mu\nu}$  and  $\eta_{mn}$  are the Poincaré AdS and the Minkowski metric tensors, respectively. In particular, we choose<sup>2</sup>

$$e_0^\mu = \left(\frac{z}{L}, 0, 0, 0\right), \quad e_1^\mu = \left(0, \frac{z}{L}, 0, 0\right), \quad e_2^\mu = \left(0, 0, \frac{z}{L}, 0\right). \quad (3.8)$$

The energy density as measured in such a orthonormal frame is

$$\rho = T'^{00} = \frac{z^2}{L^2} T'_{tt}, \quad (3.9)$$

and the components of the Poynting vector  $\vec{s} = (s_z, s_x, s_\varphi)$  are

$$s_z = T'^{01} = -\frac{z^2}{L^2} T'_{tz}, \quad s_x = T'^{02} = -\frac{z^2}{L^2} T'_{tx}, \quad s_\varphi = 0. \quad (3.10)$$

In figure 4 and 5 we show the numerical results for the energy density and the energy flux into the bulk at fixed time.

The pictures clearly illustrate how the energy density, initially localised near the AdS boundary, spreads into the bulk. The energy distribution resembles a pointlike particle only at early times, while at late times the energy is spread along a spherical wavefront. At  $t = 0$  all the components of the Poynting vector vanish, implying that there is no energy flux at initial time.

## 4 Expectation values of local operators

To understand the physical interpretation on the boundary CFT, it is useful to study the expectation values of some important local operators. In particular, in this section we will focus on expectation values of scalar operators, global  $SU(2)$  currents and energy-momentum tensor. The details depend on the boundary conditions chosen for the scalar field  $\phi^a$ . In general, the boundary energy-momentum tensor  $T_{mn}$  is not conserved because the external sources perform work on the system. With a particular choice of multitrace deformation, see eq. (4.14), the system is isolated and  $T_{mn}$  is conserved.

### 4.1 Boundary conditions for the scalar

In the AdS/CFT correspondence, the asymptotic behaviour of the bulk fields is dual to the source and expectation values of operators in the CFT. For this reason, we will focus on asymptotics of the scalar field  $\phi^a$  nearby the boundary. In global AdS, the direction  $n^a$  of  $\phi^a$  in the internal  $SU(2)$  space is given by eq. (2.16). In Poincaré patch, by performing the coordinate transformation in eq. (3.3) we find that, nearby the boundary at  $z = 0$ ,

$$n^a = \frac{1}{\omega^{1/2}} \left( -2Ax \cos(\varphi), -2Ax \sin(\varphi), A^2 + t^2 - x^2 \right) + O(z^2), \quad (4.1)$$

where, for convenience, we introduce the quantity  $\omega(x, t)$  that appears in many subsequent expressions

$$\omega(x, t) = A^4 + 2A^2(t^2 + x^2) + (t^2 - x^2)^2. \quad (4.2)$$

---

<sup>2</sup>In this section, the Minkowski indices  $m, n$  take the values 0, 1, 2, 3, while the curved spacetime indices are  $t, z, x, \varphi$ .

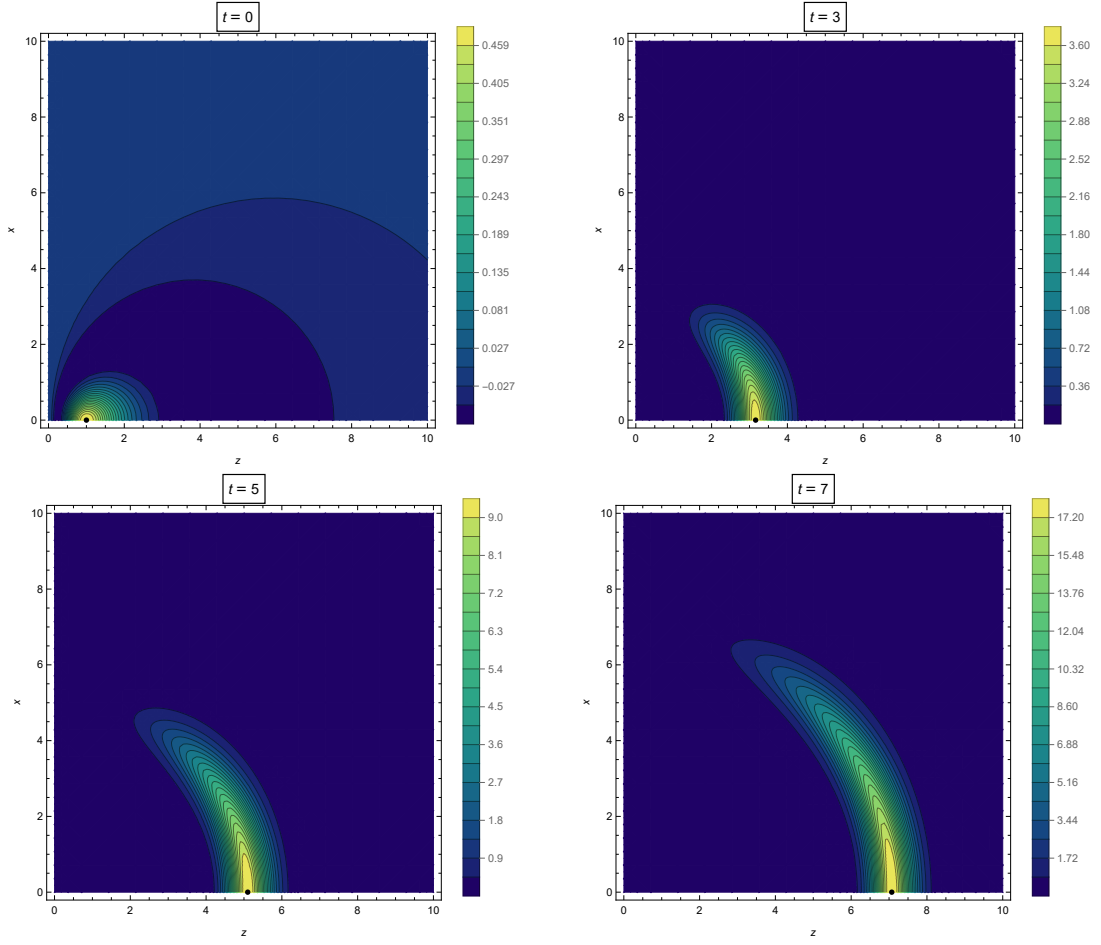


Figure 4: Contour lines of constant energy density for fixed time. The monopole center is represented by the black spot. The numerical values  $A = 1$  and  $L = 1$  have been chosen.

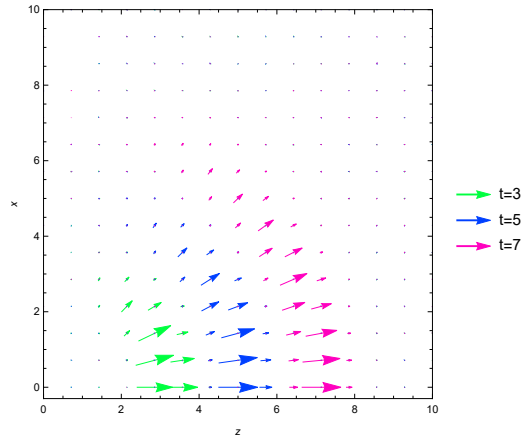


Figure 5: Direction of the bulk Poynting vector for fixed time. The numerical values  $A = 1$  and  $L = 1$  have been chosen.

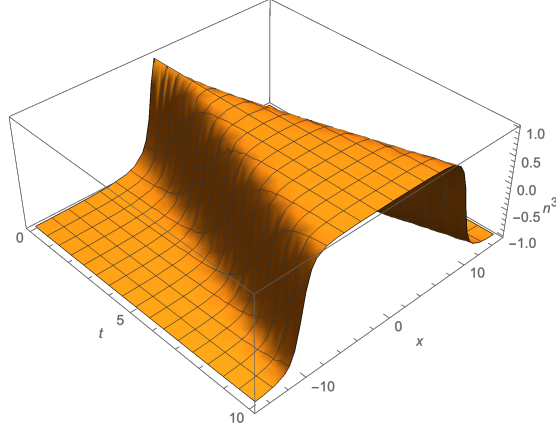


Figure 6: Value of  $n^3$  as a function of  $(t, x)$  for  $A = 1$ . Negative values of the radial cylindrical coordinate  $x$  correspond to  $\varphi \rightarrow -\varphi$ .

The core of the quench can be thought of as localised at

$$x = \sqrt{t^2 + A^2}, \quad (4.3)$$

which, at large  $t$ , coincides with good approximation with the lightcone of the origin  $x = t$ . For the value in eq. (4.3), the adjoint scalar field points in the direction  $n = n^a \sigma^a$  given by

$$n = -(\sigma_1 \cos \varphi + \sigma_2 \sin \varphi). \quad (4.4)$$

The scalar points along the  $\sigma_3$  direction inside the lightcone, and along the  $-\sigma_3$  outside the lightcone, see figure 6. As we will see later, at large  $t$ , the absolute value of the scalar field is peaked on  $x$  given by eq. (4.3), and is almost zero both inside and outside the lightcone.

The configuration at  $t = 0$  resembles a baby skyrmion, with a field pointing along  $\sigma_3$  in the core and along  $-\sigma_3$  far away (actually, it is not a skyrmion because the VEV tends to zero at infinity). As time increases, this configuration expands along the lightcone. At large time we end up with two region of vacuum (inside and outside lightcone) separated by an expanding shell of energy.

In order to extract the sources and the expectation values of the local operator triggering the quench, it is useful to expand the change of variables in eq. (3.3) nearby the boundary. The global AdS radial coordinate reads

$$r = \frac{a}{z} + O(z), \quad a = \frac{\omega^{1/2}}{2A}. \quad (4.5)$$

By means of eq. (4.5), we obtain the boundary expansion of  $H(r)$

$$H = \frac{\alpha_H}{r} + \frac{\beta_H}{r^2} + O(r^{-3}) = \tilde{\alpha}_H z + \tilde{\beta}_H z^2 + O(z^3), \quad (4.6)$$

where

$$\tilde{\alpha}_H = \frac{\alpha_H}{a} = \alpha_H \frac{2A}{\omega^{1/2}}, \quad \tilde{\beta}_H = \frac{\beta_H}{a^2} = \beta_H \frac{4A^2}{\omega}. \quad (4.7)$$

A plot of  $\tilde{\alpha}_H$  and  $\tilde{\beta}_H$  is shown in figure 7. It is interesting to note that

$$\frac{\tilde{\beta}_H}{\tilde{\alpha}_H^2} = \frac{\beta_H}{\alpha_H^2} = \kappa, \quad (4.8)$$

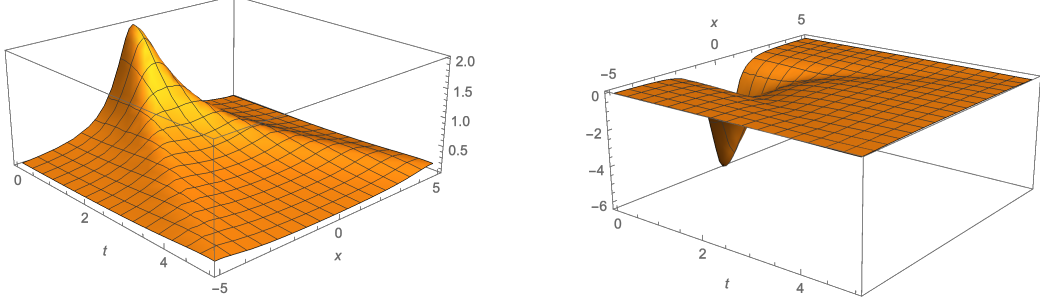


Figure 7: The quantities  $\tilde{\alpha}_H$  (left) and  $\tilde{\beta}_H$  (right) as a function of  $(t, x)$ . Here we set  $A = 1$ ,  $\alpha_H = 1$  and we use the relations in eq. (2.19), valid for small backreaction.

where  $\kappa$  is a constant. In the limit of small backreaction, from eq. (2.19) we find

$$\kappa = -\frac{\pi}{2\alpha_H}. \quad (4.9)$$

Combining eqs. (4.1) and (4.6), the expansion of  $\phi^a$  nearby the Poincaré patch boundary is

$$\phi^a = \frac{H(z)}{L} n^a = \frac{1}{L} \left( \tilde{\alpha}^a z + \tilde{\beta}^a z^2 + O(z^3) \right), \quad \tilde{\alpha}^a = n^a \tilde{\alpha}_H, \quad \tilde{\beta}^a = n^a \tilde{\beta}_H. \quad (4.10)$$

As for the global AdS case, we can consider several quantisations for the scalar field  $\phi^a$ :

- the Dirichlet condition, where  $\tilde{\alpha}_H$  corresponds to the source and  $\tilde{\beta}_H$  to the VEV

$$J_D^a = \tilde{\alpha}^a, \quad \langle \mathcal{O}_2^a \rangle = \tilde{\beta}^a. \quad (4.11)$$

- the Neumann condition, where  $-\tilde{\beta}_H$  corresponds to the source and  $\tilde{\alpha}_H$  to the VEV

$$J_N^a = -\tilde{\beta}^a, \quad \langle \mathcal{O}_1^a \rangle = \tilde{\alpha}^a. \quad (4.12)$$

- the multitrace deformation, where the boundary dual is deformed by the action term

$$S_{\mathcal{F}} = \int d^3x \sqrt{-h} [J_{\mathcal{F}}^a \tilde{\alpha}^a + \mathcal{F}(\tilde{\alpha}^a)], \quad J_{\mathcal{F}}^a = -\tilde{\beta}^a - \frac{\partial \mathcal{F}}{\partial \tilde{\alpha}^a}, \quad (4.13)$$

and  $\langle \mathcal{O}_1^a \rangle = \tilde{\alpha}^a$ .

All these boundary conditions correspond in general to a monopole in presence of external time-dependent sources. Among such possible choices of boundary conditions, it is interesting to consider the multitrace deformation with

$$\mathcal{F}_{\kappa}(\tilde{\alpha}^a) = -\frac{\kappa}{3} (\tilde{\alpha}^a \tilde{\alpha}^a)^{3/2} = -\frac{\kappa}{3} \tilde{\alpha}_H^3. \quad (4.14)$$

In this case, the monopole is a solution with a vanishing source, because it satisfies

$$\tilde{\beta}^a = -\frac{\partial \mathcal{F}}{\partial \tilde{\alpha}^a}, \quad (4.15)$$

as can be checked from eq. (4.8).

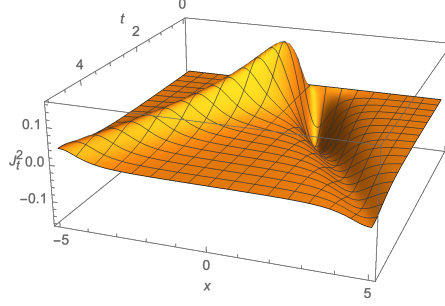


Figure 8: Charge density of the second component of isospin  $J_t^2$  as a function of  $(t, x)$  for  $\varphi = 0$  (positive  $x$ ) and  $\varphi = \pi$  (negative  $x$ ). We set  $A = 1$ ,  $\alpha_H = 1$  and  $e = 1$  and we use the relations in eq. (2.19), valid for small backreaction. The peak and the pit correspond to positive and negative sign global charges, which are taken apart from each other by the quench.

## 4.2 The boundary global currents

Our monopole ansatz in global AdS is given by eq. (2.15), with boundary conditions in eq. (2.17) and with  $\alpha_F = 0$ . As a consequence, we deduce that in Poincaré patch the gauge field  $A_\mu^a$  vanishes at the boundary  $z = 0$ . In other words, if the sources for the global symmetries are set to zero in global AdS, they also vanish after the change of coordinates leading to the Poincaré patch.

From the order  $z$  terms in the boundary expansion of  $A_\mu^a$  we can extract the expectation value of the three currents  $J_t^a$

$$\begin{aligned} \langle J_t^1 \rangle &= \frac{8A^2\beta_F}{\omega^{3/2}} \left( tx \sin(\varphi), -\frac{1}{2} \sin(\varphi) (A^2 + t^2 + x^2), -\frac{1}{2} x \cos(\varphi) (A^2 + t^2 - x^2) \right), \\ \langle J_t^2 \rangle &= \frac{8A^2\beta_F}{\omega^{3/2}} \left( -tx \cos(\varphi), \frac{1}{2} \cos(\varphi) (A^2 + t^2 + x^2), -\frac{1}{2} x \sin(\varphi) (A^2 + t^2 - x^2) \right), \\ \langle J_t^3 \rangle &= \frac{8A^2\beta_F}{\omega^{3/2}} (0, 0, -Ax^2), \end{aligned} \quad (4.16)$$

where  $x^l = (t, x, \varphi)$  are the boundary spacetime coordinates, and  $a = 1, 2, 3$  is the  $SU(2)$  global index. Plots of the charge density  $J_t^2$  is shown in figure 8.

It is interesting to compare the direction in the  $SU(2)$  space of the current expectation value with the direction of the scalar expectation value  $n^a$ . We find that the expectation value of the global current is always orthogonal to the direction of the scalar expectation value in the isospin space

$$\langle J_m^a \rangle n^a = 0. \quad (4.17)$$

So the quench breaks all the three global symmetry group generators. This is true just on top of the "lightcone" in eq. (4.3); inside and outside this surface both the scalar and the current expectation values tend to zero and the  $SU(2)$  global symmetry of the boundary theory is unbroken.

## 4.3 The boundary energy-momentum tensor

For illustrative purposes, we will compare the result with the one obtained for a quench modelled by a falling black hole, studied in [31]. In this case the metric is

$$ds^2 = L^2 \left( - \left( 1 + r^2 - \frac{M}{r} \right) d\tau^2 + \frac{dr^2}{1 + r^2 - \frac{M}{r}} + r^2 (d\theta^2 + \sin^2 \theta d\varphi^2) \right), \quad (4.18)$$

where  $M$  is a dimensionless parameter proportional to the black hole mass. In order to find the quench background, we apply the change of variables in eq. (3.2). Then, to extract the energy-momentum tensor with the method in [59], it is convenient to pass to Fefferman-Graham (FG) coordinates. Details of the calculation are in appendix C.1, where expressions for all the components of the energy-momentum tensor can also be found, see eq. (C.7). In particular, the energy density is

$$T_{tt}^{(BH)} = \frac{A^3 L^2 M}{\pi G} \frac{\omega + 6t^2 x^2}{\omega^{5/2}}. \quad (4.19)$$

The energy-momentum tensor is conserved and traceless, and the total energy is

$$\mathcal{E}^{(BH)} = \frac{M L^2}{2 G A}. \quad (4.20)$$

In the falling monopole case a more accurate discussion is needed, since the boundary energy-momentum tensor depends on the details of the boundary conditions of bulk fields. We first focus on Dirichlet boundary conditions [60]. Starting from the backreacted metric in eq. (2.21), we apply the change of variables in eq. (3.2). The intermediate metric expression is a bit cumbersome, so in appendix C.2 we just specify the coordinates expansion that puts it in the FG form. All the non-vanishing components of the energy-momentum tensor  $T_{mn}^{(D)}$  obtained from such a metric are given in eq. (C.10). The energy density is:

$$\begin{aligned} T_{tt}^{(D)} &= \frac{A^3}{3\pi G \omega^{5/2}} [48\pi G \alpha_H \beta_H x^2 t^2 + (8\pi G \alpha_H \beta_H - 3g_3 L^2)(\omega + 6t^2 x^2)] \\ &= 2\pi \alpha_H^2 A^3 \frac{\omega + 2t^2 x^2}{\omega^{5/2}}, \end{aligned} \quad (4.21)$$

where in the second line we have inserted the analytic approximations for small backreaction in eqs. (2.19) and (2.27). In this limit, the total energy is

$$\mathcal{E}^{(D)} = \frac{\pi^2 \alpha_H^2}{A} \left( 1 - \frac{2}{3} \frac{t^2}{A^2 + t^2} \right). \quad (4.22)$$

The energy is a decreasing function of time, meaning that the Dirichlet boundary conditions absorb energy from the bulk. The non-conservation of energy motivates the investigation of a different quantisation.

A changing of the quantisation conditions causes a shift of  $T_{mn}^{(D)}$  by finite parts (see e.g. [58]). Here we specialise to a class of multitrace deformations that do not break the  $SU(2)$  global symmetry. Assuming that

$$\tilde{\alpha}^a = n^a \tilde{\alpha}_H, \quad \tilde{\beta}^a = n^a \tilde{\beta}_H, \quad (4.23)$$

which is true for the monopole, we can write the source as

$$J_{\mathcal{F}}^a = n^a J_{\mathcal{F}}. \quad (4.24)$$

As a function  $\mathcal{F}$  parameterising the multitrace deformation we choose

$$\mathcal{F}(\tilde{\alpha}^a) = \mathcal{F}(\tilde{\alpha}^a \tilde{\alpha}^a) = \mathcal{F}(\alpha_H). \quad (4.25)$$

The current can be written in terms of  $\tilde{\alpha}_H, \tilde{\beta}_H$  as follows

$$J_{\mathcal{F}} = -\tilde{\beta}_H - \mathcal{F}'(\tilde{\alpha}_H). \quad (4.26)$$

The energy-momentum tensor, (see appendix C.3 for further details) is

$$T_{ij}^{(\mathcal{F})} = T_{ij}^{(D)} + \eta_{ij}[\mathcal{F}(\tilde{\alpha}_H) - \tilde{\alpha}_H \tilde{\beta}_H - \mathcal{F}'(\tilde{\alpha}_H) \tilde{\alpha}_H]. \quad (4.27)$$

Note that this result also applies to the Neumann conditions, that can be seen as a multitrace deformation with  $\mathcal{F} = 0$ . If we instead specialise to  $\mathcal{F} = \mathcal{F}_\kappa$ , see eq. (4.14), the external source is zero and the energy-momentum tensor is conserved. Moreover, an explicit computation reveals that the energy-momentum tensor has the same functional form as the one for the falling BH:

$$T_{ij}^{(\kappa)} = \frac{16\pi G \alpha_H \beta_H - 3L^2 g_3}{3L^2 M} T_{ij}^{(BH)}. \quad (4.28)$$

Using the analytic values for small backreaction of  $\beta_H$  and  $g_3$  in eqs. (2.19) and (2.27), we find

$$T_{ij}^{(\kappa)} = \frac{2\pi^2 G \alpha_H^2}{3L^2 M} T_{ij}^{(BH)}, \quad T_{tt}^{(\kappa)} = \frac{2\pi \alpha_H^2 A^3}{3} \frac{\omega + 6t^2 x^2}{\omega^{5/2}}. \quad (4.29)$$

The total energy is

$$\mathcal{E}^{(\kappa)} = \frac{\pi^2 \alpha_H^2}{3A}. \quad (4.30)$$

As apparent from eq. (4.28), the energy-momentum tensor is not a probe enough precise to distinguish between a falling monopole or a falling black hole in the bulk. In the next section, we will see that the entanglement entropy of these two falling objects behaves instead in a radically different way.

## 5 Holographic entanglement entropy

In this section we will study the effect of the leading-order backreaction on holographic entanglement entropy. It is useful to consider  $\epsilon$  as defined in eq. (2.25) as an expansion parameter. In the asymptotically global AdS case, the metric at the leading order in  $\epsilon$  is

$$ds^2 = L^2 \left( -(1+r^2) [1 + \epsilon(h_\epsilon + g_\epsilon)] d\tau^2 + [1 + \epsilon(h_\epsilon - g_\epsilon)] \frac{dr^2}{1+r^2} + r^2(d\theta^2 + \sin^2 \theta d\varphi^2) \right), \quad (5.1)$$

where  $h_\epsilon$  and  $g_\epsilon$  are given by eq. (2.26). We will be interested in the evolution of entanglement entropy for the quench in Poincaré patch, so we apply the change of variables in eq. (3.3), obtaining a time-dependent background.

The metric tensor can be written as follows

$$g_{\mu\nu} = g_{\mu\nu}^{(0)} + \epsilon g_{\mu\nu}^{(1)} + O(\epsilon^2), \quad \epsilon = \frac{\pi G \alpha_H^2}{L^2}. \quad (5.2)$$

Given a codimension-two surface  $x^\mu(y^\alpha)$  parameterised with coordinates  $y^\alpha = (y^1, y^2)$ , the induced metric is

$$G_{\alpha\beta} = \frac{\partial x^\mu}{\partial y^\alpha} \frac{\partial x^\nu}{\partial y^\beta} g_{\mu\nu}. \quad (5.3)$$

Such an induced metric can also be expanded as a power series in  $\epsilon$

$$G_{\alpha\beta} = G_{\alpha\beta}^{(0)} + \epsilon G_{\alpha\beta}^{(1)} + O(\epsilon^2), \quad G_{\alpha\beta}^{(k)} = \frac{\partial x^\mu}{\partial y^\alpha} \frac{\partial x^\nu}{\partial y^\beta} g_{\mu\nu}^{(k)}, \quad k = 0, 1. \quad (5.4)$$

We can compute the change of area of the Ryu-Takayanagi (RT) surface at the leading order in  $\epsilon$ , as in [31]. To this purpose, we can expand the determinant of the metric in the area functional. The first order term of this expansion is

$$\Delta \mathcal{A} = \frac{\epsilon}{2} \int d^2 y \sqrt{G^{(0)}} \text{Tr} \left[ G^{(1)} (G^{(0)})^{-1} \right]. \quad (5.5)$$

It is important to note that, at first order, it is enough to work with the unperturbed RT surface  $x^\mu(y^\alpha)$ , which simplifies the computation a lot. The difference in entropy between the excited state and the vacuum at the leading order is proportional to eq. (5.5)

$$\Delta S = \frac{\Delta \mathcal{A}}{4G}. \quad (5.6)$$

We will apply this procedure to various examples of subregions.

### 5.1 Disk centered at the origin

We take as a boundary subregion a disk of radius  $l$  centered at  $x = 0$  and lying at constant time  $t$ . The RT surface in unperturbed Poincaré patch of  $\text{AdS}_4$  is the half sphere

$$z = \sqrt{l^2 - x^2}. \quad (5.7)$$

From eqs. (5.5) and (5.1) we obtain

$$\Delta S(l, t) = \frac{\pi^2 \alpha_H^2}{4} \frac{1}{l} \int_0^l \frac{(h_\epsilon - g_\epsilon) x^3}{(l^2 - x^2)^{3/2}} \frac{\omega(l, t)}{(A^2 - l^2 + t^2)^2 + 4A^2 x^2} dx, \quad (5.8)$$

where  $\omega$  is defined in eq. (4.2). The functions  $h_\epsilon$  and  $g_\epsilon$  depend on the variable  $r$ , which on top of the RT surface reads

$$r = \frac{\sqrt{(A^2 - l^2 + t^2)^2 + 4A^2 x^2}}{2A\sqrt{l^2 - x^2}}. \quad (5.9)$$

For the entropy, the  $A$  dependence can be completely reabsorbed by the following rescaling of the quantities  $l$ ,  $x$  and  $t$

$$l \rightarrow \frac{l}{A}, \quad x \rightarrow \frac{x}{A}, \quad t \rightarrow \frac{t}{A}. \quad (5.10)$$

For this reason, the numerical analysis has been performed for  $A = 1$  without loss of generality. Numerical results are shown in figure 9. We find that  $\Delta S$  is always negative, meaning that the perturbed entanglement entropy is always smaller than the vacuum value. We can think of the quench as a region of spacetime where a condensate (which breaks a global symmetry on the boundary, as in holographic superconductors [61]) is localised. A lower entropy fits with the intuition that some degrees of freedom have condensed [53] and so there should be fewer of them compared to the vacuum (which has zero scalar expectation value).

Analytic results can be found in some regimes. Nearby the boundary  $r \rightarrow +\infty$ , we can use the expansion

$$h_\epsilon = -\frac{2}{r^2} + \dots, \quad g_\epsilon = \frac{2}{r^2} + \dots. \quad (5.11)$$

Since the minimal  $r$  on the RT surface is given by eq. (5.9) with  $x = 0$ , this expansion will be valid in the whole integration region in eq. (5.8) in the regime

$$|A^2 + t^2 - l^2| \gg 2lA. \quad (5.12)$$

Equation (5.8) can then be evaluated explicitly

$$\Delta S = -\pi^2 \alpha_H^2 \left[ \left( \frac{Al}{\sqrt{\omega(l, t)}} + \frac{\sqrt{\omega(l, t)}}{4Al} \right) \tanh^{-1} \left( \frac{2Al}{\sqrt{\omega(l, t)}} \right) - \frac{1}{2} \right]. \quad (5.13)$$

We can specialise the approximation in eq. (5.12) to the following situations:



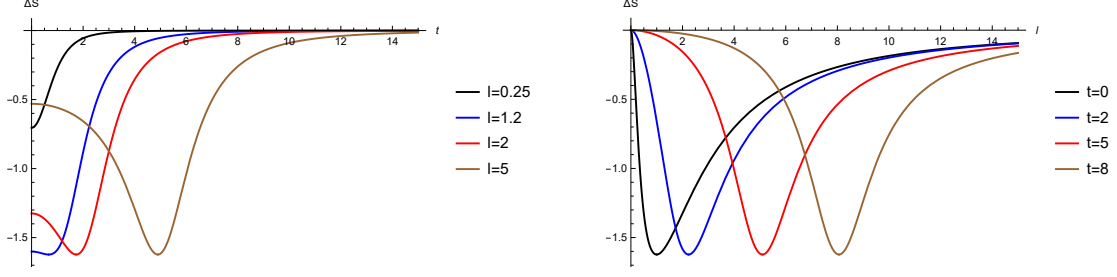


Figure 9: Left: time dependence of  $\Delta S$  for a spherical subregion with fixed radius  $l$  centered at the origin of the quench. Right: dependence of  $\Delta S$  at fixed  $t$  as a function of  $l$ . The numerical values  $\alpha_H = 1$ ,  $A = 1$  are used.

- small  $l \ll A$

$$\Delta S = -\frac{8}{3}\pi^2 \alpha_H^2 \frac{A^2 l^2}{(A^2 + t^2)^2}. \quad (5.14)$$

- large  $t \gg A$  and  $t \gg l$

$$\Delta S = -\frac{8}{3}\pi^2 \alpha_H^2 \frac{l^2 A^2}{t^4}. \quad (5.15)$$

- $t = 0$  and  $l \gg A$

$$\Delta S = -\frac{8}{3}\pi^2 \alpha_H^2 \frac{A^2}{l^2}. \quad (5.16)$$

It is useful to note that, for given  $(l, t)$ , the minimal surfaces in eq. (5.7) in the Poincaré patch are mapped by eq. (3.3) to constant  $\tau$  surfaces in global AdS. These surfaces are attached at  $r \rightarrow \infty$  to a circle with constant  $\theta = \theta_0$ , where

$$\theta_0(l, t) = \tan^{-1} \left( \frac{2Al}{l^2 - t^2 - A^2} \right), \quad (5.17)$$

which corresponds to a parallel on the  $S^2$  boundary. This shows that  $\Delta S(l, t)$  is a function just of the combination in eq. (5.17).

The RT surfaces with

$$l = l_0 = \sqrt{t^2 + A^2} \quad (5.18)$$

corresponds to a parallel with  $\theta_0 = \pi/2$ . These surfaces are special, because they lie on the equator of  $S^2$ . Due to symmetry, we conclude that the RT surface at  $l = l_0$  has either the maximal or the minimal  $\Delta S$ . For the monopole case, we know that  $\Delta S$  is negative and close to zero for  $t \rightarrow 0$  and large  $l$ . So we expect that  $l = l_0$  is a minimum of  $\Delta S$ , as also confirmed by the numerics in figure 9.

For  $l = l_0$ ,  $\Delta S$  can be computed exactly:

$$\Delta S_0 = \Delta S(l_0) = \frac{\pi^2 \alpha_H^2}{4} \int_0^\infty (h_\epsilon - g_\epsilon) \frac{r}{\sqrt{1+r^2}} dr = -\Upsilon \frac{\pi^2 \alpha_H^2}{4}, \quad (5.19)$$

where

$$\Upsilon = 6\pi - 12 - 8\pi \beta(2) + 14\zeta(3) \approx 0.658. \quad (5.20)$$

In this expression,  $\beta(2) \approx 0.916$  is the Catalan constant and  $\zeta$  is the Riemann zeta function.

Summarising, the entropy of the disk with radius  $l_0 = \sqrt{t^2 + A^2}$  remains constant as a function of the time  $t$  and equal to the minimum  $\Delta S_0$ . This can be heuristically justified as follows. At large  $t$ , the bound from causality on the speed of entanglement propagation is saturated:  $\Delta S$ , which originated at  $t = 0$  from a region nearby  $x = 0$ , spreads at the speed of light. At small  $t$ , the speed of propagation is smaller, because at  $t \rightarrow 0$  also the matter of the quench has zero velocity: entanglement spreads with matter.

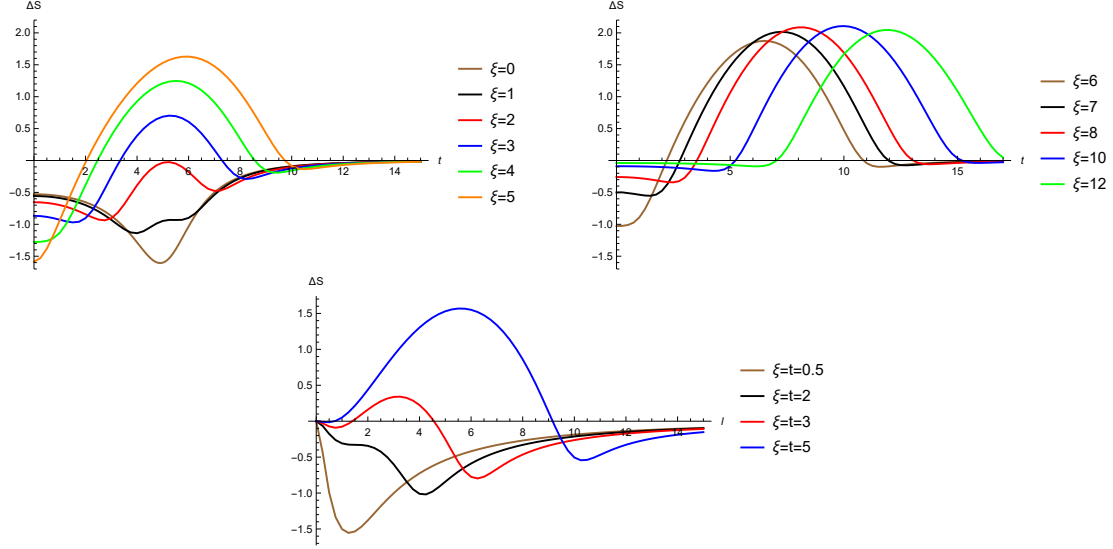


Figure 10: Left and right: Time dependence of  $\Delta S$  for a disk-shaped subregion of radius  $l = 5$  centered at  $(x_1, x_2) = (\xi, 0)$  for different values of  $\xi$ . For large  $\xi$ , the maximum is reached for  $t \approx \xi$ . Bottom: Plot of  $\Delta S$  as a function of  $l$  for a translated disk-shaped subregion, for various values of  $t = \xi$ . Numerical values  $\alpha_H = 1$ ,  $A = 1$  have been fixed.

## 5.2 Translated disk

For convenience, we introduce

$$\vec{x} = (x_1, x_2) = (x \cos \varphi, x \sin \varphi) . \quad (5.21)$$

We now consider as subregion a disk of radius  $l$  centered at  $(x_1, x_2) = (\xi, 0)$  and lying at constant time  $t$ . The corresponding RT surface in unperturbed Poincaré  $\text{AdS}_4$  is the translated half sphere

$$z = \sqrt{l^2 - (x_1 - \xi)^2 - x_2^2} . \quad (5.22)$$

In appendix D.1 we write the explicit integral for the first-order correction to the holographic entanglement entropy. It is convenient to rescale spatial and time coordinates as in eq. (5.10), with  $\xi \rightarrow \xi/A$  as well. Numerical results can be obtained for arbitrary radius  $l$ , see figure 10.

In the regime of small  $l$ , the RT surface stays at large  $r$ , so we can use the expansion (5.11) and a compact expression can be found

$$\Delta S(l, t, \xi) = -\frac{8}{3}\pi^2 \alpha_H^2 \frac{A^2 l^2}{A^4 + 2A^2(\xi^2 + t^2) + (t^2 - \xi^2)^2} . \quad (5.23)$$

This shows that  $\Delta S$  is always negative for disks with small radius  $l$ . The entanglement entropy of small disks is then dominated by the negative contribution due to the scalar condensation.

At large  $l \gg \xi$ , the subregion is, with good approximation, a disk centered at  $\xi \approx 0$ , and so, from the results of the previous section, we expect a negative  $\Delta S$ . For intermediate  $l$ , the quantity  $\Delta S$  can become positive, see figure 10. In this regime we can interpret the positive contribution to  $\Delta S$  as due to quasiparticles.

Free quasiparticles provide a simple model of entanglement propagation [9]. In this picture, the quench is assumed to create many copies of Einstein-Podolsky-Rosen (EPR)

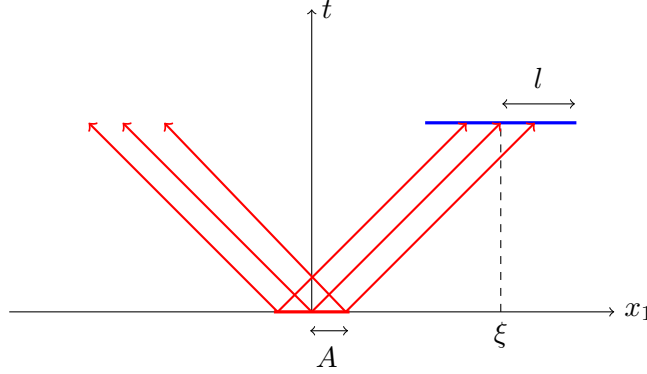


Figure 11: In the quasiparticle model, the quench creates EPR pairs of entangled quasiparticles which subsequently propagate without interactions. When just one of the quasiparticles belonging to an EPR pair is inside the blue region, the entanglement entropy of the region increase.

pairs, which then propagate without interactions, see figure 11. When just one of the entangled particles in an EPR pair is inside a given region, there is a positive contribution to the entanglement entropy. This model can reproduce several aspects of the spread of entanglement in global and local quenches. Models with interacting quasiparticles have also been studied [20]. In all these models, the contribution of the excitations to the entanglement entropy is always positive. In the monopole quench, there is also a negative contribution to the entanglement entropy due to the scalar condensate. In general, we expect that there is a competition between the quasiparticle and the condensate contribution, which is responsible for the change of sign of the entanglement entropy of the translated disk region.

### 5.3 Half-plane region

We take as a boundary subregion the half-plane  $x_1 \geq 0$  at constant time  $t$ . The unperturbed RT is the bulk surface at  $x_1 = 0$  and constant time  $t$ . A convenient choice of parameters is

$$y^\alpha = (z, x_2) . \quad (5.24)$$

Details of the calculations are in appendix D.2. From the closed-form expression, we deduce that the entropy variation  $\Delta S$  is a function of  $t/A$ . Numerical result is shown in figure 12.

For  $t = 0$ , the entropy is given by  $\Delta S_0$  in eq. (5.19). This is because, due to the change of variables in eq. (3.3), the  $t = 0$  plane with  $x_1 = 0$  (which corresponds to  $\varphi = \pm\pi/2$ ) is mapped in global AdS to a disk with  $\tau = 0$  and constant  $\varphi = \pm\pi/2$ . Then, an explicit computation easily leads to the same entropy as in (5.19).

At large  $t$ , from the analysis in appendix D.2, we find that  $\Delta S$  scales in a linear way with time, i.e.

$$\Delta S = K \alpha_H^2 \frac{t}{A}, \quad K \approx 0.636 . \quad (5.25)$$

An exact expression for  $K$  is given in eq. (D.13). This is consistent with numerical results, shown in figure 12. We emphasise that this result is valid only in the regime where we can trust our perturbative calculation in the parameter  $\epsilon$ . At very large  $t$ , we expect that the large backreaction effects spoil the results in eq. (5.25). A linear behaviour at large  $t$  is also realised for the perturbative entropy in the case of a falling black hole in AdS<sub>4</sub> [38].

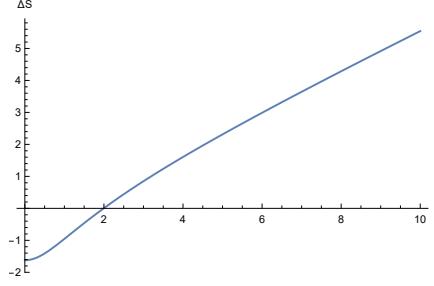


Figure 12: Time dependence of  $\Delta S$  for the half-plane subregion. The numerical values  $\alpha_H = 1$ ,  $A = 1$  have been chosen.

The numerical plot in figure 12 is consistent with both the  $t = 0$  and large  $t$  analytical calculations. At  $t = 0$ ,  $\Delta S$  is negative, in agreement with the expectation that the condensate decreases the entanglement entropy. Immediately after  $t = 0$ , the quantity  $\Delta S$  enters in a linear growth regime and becomes positive around  $t \approx 2A$ . This linear behaviour is similar to the one of the black hole quench and we expect that it is due to the contribution of quasiparticles.

#### 5.4 Comparison with the BH quench

In the case of a falling black hole in  $\text{AdS}_4$ , the perturbative entropy for a centered disk is

$$\Delta S^{(BH)} = \frac{\pi M L^2}{4G A l} \left( \frac{l^4 - 2l^2 t^2 + (A^2 + t^2)^2}{\sqrt{l^4 + 2l^2 (A^2 - t^2) + (A^2 + t^2)^2}} - |t^2 + A^2 - l^2| \right), \quad (5.26)$$

where  $M$  is the mass parameter, as defined in eq. (4.18). In this case,  $\Delta S^{(BH)}$  is always positive and has a maximum for  $l = l_0 = \sqrt{t^2 + A^2}$ . The First Law of Entanglement Entropy (FLEE) [62] is valid in the regime of small  $l$ :

$$\Delta S = \frac{\Delta E}{T_E}, \quad T_E = \frac{2}{\pi l}, \quad (5.27)$$

where  $T_E$  is the entanglement temperature and  $\Delta E$  is the energy.

FLEE is generically invalidated in the case of backgrounds with scalars, because the Fefferman-Graham expansion of the metric does not start at order  $z^d$  [63, 64], where  $d$  is the dimension of the spacetime boundary. Indeed, as can be checked from eq. (5.23), FLEE is not satisfied for the monopole quench background. The behaviour of  $\Delta S$  for small  $l$  in eq. (5.23) is rather different from the FLEE regime. In particular:

- $\Delta S$  is negative;
- the quantity  $\Delta S$  scales as  $l^2$ , and not as  $l^3$  as predicted by FLEE;
- there is no choice of boundary conditions for which the energy  $\Delta E$  is proportional to  $\Delta S$ .

The FLEE can be derived from the notion of relative entropy [6, 63], which is a quantity that measures how far is a density matrix  $\rho$  from a reference density matrix  $\sigma$ :

$$S(\rho||\sigma) = \text{Tr}(\rho \log \rho) - \text{Tr}(\rho \log \sigma). \quad (5.28)$$

As a general property,  $S(\rho||\sigma)$  is positive definite and it vanishes if and only if  $\rho = \sigma$ . The relative entropy can be written as

$$S(\rho||\sigma) = \Delta\langle\mathcal{K}_\sigma\rangle - \Delta S, \quad (5.29)$$

where  $\mathcal{K}_\sigma$  is the modular Hamiltonian of the density matrix  $\sigma$

$$\mathcal{K}_\sigma = -\log \sigma. \quad (5.30)$$

From positivity of relative entropy we get the relation

$$\Delta\langle\mathcal{K}_\sigma\rangle \geq \Delta S. \quad (5.31)$$

The modular Hamiltonian operator  $\mathcal{K}_\sigma$  for a spherical domain with radius  $l$  in the vacuum state of a  $d$ -dimensional CFT can be expressed [65] in terms of the energy momentum operator as follows

$$\mathcal{K}_\sigma = 2\pi \int_{\text{sphere}} d^{d-1}\vec{x} \frac{l^2 - x^2}{2l} T_{tt}(\vec{x}), \quad (5.32)$$

where  $x = |\vec{x}|$ . In the limit of small spherical subregion and in  $d = 3$ , we find

$$\Delta\langle\mathcal{K}_\sigma\rangle = \frac{\pi l}{2} \Delta E, \quad (5.33)$$

so the FLEE in eq. (5.27) follows from the saturation of the identity (5.31), i.e.

$$\Delta\langle\mathcal{K}_\sigma\rangle = \Delta S. \quad (5.34)$$

If we consider two nearby density matrices, i.e.

$$\sigma = \rho_0, \quad \rho = \rho_0 + \varepsilon \rho_1 + \mathcal{O}(\varepsilon^2), \quad (5.35)$$

where  $\varepsilon$  is an expansion parameter, the relative entropy scales with  $\varepsilon$  as follows

$$S(\rho||\sigma) = \mathcal{O}(\varepsilon^2). \quad (5.36)$$

Since the  $\mathcal{O}(\varepsilon)$  contribution to relative entropy vanishes, there is a general expectation [63] that for small deformations eq. (5.31) is saturated. However, the question if FLEE is satisfied in quantum field theory is subtle: there the density matrix  $\rho$  is infinite dimensional and so it is not clear, in principle, when a perturbation might be considered small.

## 6 Conclusions

In this paper, we studied a magnetic monopole solution in the static global  $\text{AdS}_4$  setup introduced in [51]. The boundary conditions of the monopole are specified by the parameter  $\alpha_H$ , which in the multitrace quantisation is proportional to the VEV of the scalar operator in the boundary CFT. We found an approximate analytic solution for the monopole in the regime of small  $\alpha_H$  which includes the leading-order backreaction on the metric. By using the map introduced in [52], the static monopole in global  $\text{AdS}_4$  is mapped into a falling monopole in the Poincaré patch. This bulk configuration is dual to a local quench on the CFT side. The expectation values of local operators depend on the choice of the boundary conditions. With Dirichlet or Neumann conditions, the falling monopole is dual to a field theory with a time-dependent source. With the special choice of multitrace deformation in eq. (4.14), the monopole is dual to a field theory with zero sources. In this case, there

is no energy injection and the form of the energy-momentum tensor is the same as the one of a falling black hole [31].

The behaviour of entanglement entropy is instead rather different compared to the case of the falling black hole. For spherical regions centered on the local quench, the perturbed entanglement entropy is always less than the vacuum value, i.e.  $\Delta S \leq 0$ . This is consistent with the presence of a condensate at the core of the local quench [53].

In the case of a spherical region not centered at the origin, there is a competition in  $\Delta S$  between the negative contribution from the condensate and the positive one due to quasiparticles [9]. Depending on the radius  $l$  and on the distance  $\xi$  from the origin of the spherical region,  $\Delta S$  can be positive or negative, see figure 10. In the case of half-plane region, the negative contribution to  $\Delta S$  due to the condensate wins at early times, while the positive contribution due to quasiparticles dominates at late times (see figure 12).

For a quench dual to a falling black hole, the First Law of Entanglement Entropy (FLEE) [62] is satisfied for small subregions. For the quench dual to the monopole, we find that the FLEE is not satisfied. This is a feature shared with other AdS backgrounds which involve the backreaction of scalar bulk fields, see [63, 64]. On the field theory side, the violation of the FLEE comes from the non-saturation of the inequality in eq. (5.31). It is still an open question whether a given deformation obeys the FLEE [64] in a quantum field theory. It would be interesting to further investigate the FLEE in non-equilibrium systems, in order to understand its general validity conditions.

Analytical soliton solutions which include backreaction are quite rare in AdS spacetime. The monopole solution found in this paper can be the starting point for several further investigations. In particular, it would be interesting to study more general solitonic objects in AdS. For instance, vortex strings in AdS were considered by many authors [66–74]. A static configuration in Poincaré patch with a monopole attached to a vortex string should also be possible, as proposed in [71]: the vortex string pulls the vortex and it can counterbalance the gravitational force that makes it fall towards the center of AdS. It would be interesting to find explicit solutions for these objects and to investigate their field theory duals.

Another possible direction is the study of holographic complexity [75–77]. Quantum computational complexity is a recent quantum information entry in the holographic dictionary, which was motivated by the desire of understanding the growth of the Einstein-Rosen bridge inside the event horizon of black holes. Complexity in several examples of global and local quenches has been studied by several authors, e.g. [78–86]. It would be interesting to investigate complexity for quenches dual to a falling monopole. This analysis may give us useful insights to understand the impact of condensates on quantum complexity.

## Acknowledgments

We are grateful to Stefano Bolognesi for useful discussions. N.Z. acknowledges the Ermenegildo Zegna’s Group for the financial support.

## Appendix

### A Equations of motion

#### A.1 Coordinate $r$

In the probe approximation, the equations of motion are

$$\begin{aligned} F'' &= -F' \frac{2(1+2r^2)}{r(1+r^2)} - F \frac{-2+2r^2+3erF-e^2r^2F^2}{r^2(1+r^2)} - H^2 \frac{e(1-erF)}{r(1+r^2)}, \\ H'' &= -H' \frac{2(1+2r^2)}{r(1+r^2)} + 2H \frac{(1-erF)^2}{r^2(1+r^2)} - \frac{2H}{1+r^2}. \end{aligned} \quad (\text{A.1})$$

Including backreaction, the full set of equations of motion is

$$\begin{aligned} F'' &= -F' \frac{2(1+2r^2)}{r(1+r^2)} - \frac{g'}{g} \left( \frac{F}{r} + F' \right) - H^2 \frac{e(1-erF)}{r(1+r^2)} \frac{h}{g} \\ &\quad - F \frac{1}{r^2(1+r^2)} \left( 2r^2 + \frac{h}{g} [-2+3erF-e^2r^2F^2] \right), \\ H'' &= -H' \left( \frac{2(1+2r^2)}{r(1+r^2)} + \frac{g'}{g} \right) - \frac{h}{g} \left( -2H \frac{(1-erF)^2}{r^2(1+r^2)} + \frac{2H}{1+r^2} \right), \\ g' &= \frac{4\pi G}{L^2} h \frac{2H^2 [(2-erF)erF+r^2-1] - F^2(2-erF)^2}{r(1+r^2)} + \frac{1+3r^2}{r(r^2+1)} (h-g), \\ h' &= \frac{8\pi G}{L^2} h \left( \frac{r}{2} (H')^2 + \frac{(F+rF')^2}{r} \right). \end{aligned} \quad (\text{A.2})$$

#### A.2 Coordinate $\psi$

In the probe approximation, we find

$$\begin{aligned} F'' &= \frac{e^2F^3 + F(e^2H^2 + 2\cot^2(\psi) - 2) - 3eF^2\cot(\psi) - \cot(\psi)(eH^2 + 2F')}{\cos^2\psi}, \\ H'' &= 4 \frac{H(e^2F^2\tan(\psi) - 2eF + 2\cot(2\psi) + 2\lambda H^2\tan\psi) - H'}{\sin(2\psi)}. \end{aligned} \quad (\text{A.3})$$

Including backreaction, we get

$$\begin{aligned} F'' &= \frac{1}{g} [-e \csc\psi \sec\psi (3F^2 + H^2) h + e^2 \sec^2\psi F^3 h - F' (2g \csc\psi \sec\psi + g') \\ &\quad + F (h (2 \csc^2\psi + e^2 H^2 \sec^2\psi) - \sec\psi (2g \sec\psi + g' \csc\psi))] , \\ H'' &= \frac{1}{g} [2hH (\csc^2\psi - 2eF \csc\psi \sec\psi + \sec^2\psi (-1 + e^2F^2 + 2\lambda H^2)) \\ &\quad - (2g \csc\psi \sec\psi + g') H'] , \\ h' &= \frac{2\pi G}{L^2} h \left[ 2 (F \csc\psi \sec\psi + F')^2 + H'^2 \right] \sin 2\psi , \\ g' &= \tan\psi (3 + \cot^2\psi) (h - g) + \frac{4\pi G}{L^2} h \tan\psi [-F^2(-2\cot\psi + eF)^2 \\ &\quad + 2H^2 - 2(\cot\psi - eF)^2 H^2 - 2\lambda H^4] . \end{aligned} \quad (\text{A.4})$$

## B Abelian field strength and flux

The abelian field strength and its dual are [40]:

$$\mathcal{F}_{\mu\nu} = n^a F_{\mu\nu}^a - \frac{1}{e} \epsilon^{abc} n^a D_\mu n^b D_\nu n^c, \quad \tilde{\mathcal{F}}^{\mu\nu} \equiv \frac{1}{2} \frac{\epsilon^{\mu\nu\alpha\beta}}{\sqrt{-g}} \mathcal{F}_{\alpha\beta}, \quad (\text{B.1})$$

which satisfies

$$D_\mu \tilde{\mathcal{F}}^{\mu\nu} = \frac{4\pi}{e} k^\nu, \quad k_\mu = \frac{1}{8\pi} \epsilon_{\mu\nu\rho\sigma} \epsilon_{abc} \partial^\nu n^a \partial^\rho n^b \partial^\sigma n^c, \quad (\text{B.2})$$

where  $k_\mu$  is the topological current. The only non-vanishing component of the dual electromagnetic tensor  $\tilde{\mathcal{F}}^{\mu\nu}$  is:

$$\tilde{\mathcal{F}}^{tr} = -\frac{1}{er^2}. \quad (\text{B.3})$$

The magnetic flux on a sphere of radius  $r$  is given by Stokes theorem:

$$Q = \int_{S^2} \tilde{\mathcal{F}}^{\mu\nu} dS_{\mu\nu}, \quad dS_{\mu\nu} = n_{[\mu} r_{\nu]} r^2 \sin\theta d\theta d\phi, \quad (\text{B.4})$$

where  $n_\mu$  and  $r_\nu$  are the unit time and radial vectors, respectively. A direct computation gives:

$$Q = -\frac{8\pi}{e}. \quad (\text{B.5})$$

Note that the magnetic flux is topological and independent of the profile functions details.

## C Details of the boundary energy-momentum tensor

### C.1 Black hole

In Fefferman-Graham (FG) coordinates, the metric has the following form

$$\hat{x}^\mu = (\hat{z}, \hat{t}, \hat{x}, \hat{\varphi}) \quad ds^2 = L^2 \left( \frac{d\hat{z}^2}{\hat{z}^2} + \frac{1}{\hat{z}^2} g_{ab}(\hat{z}, \hat{x}^a) d\hat{x}^a d\hat{x}^b \right), \quad (\text{C.1})$$

where the index  $a$  runs on boundary coordinates

$$\hat{x}^a = (\hat{t}, \hat{x}, \hat{\varphi}), \quad (\text{C.2})$$

and we take  $\hat{\varphi} = \varphi$ . The FG coordinates can be built in a perturbative way nearby the boundary, i.e.

$$z = \hat{z} + \sum_{k=2}^{\infty} a_k(\hat{x}, \hat{t}) \hat{z}^k, \quad x = \hat{x} + \sum_{k=1}^{\infty} b_k(\hat{x}, \hat{t}) \hat{z}^k, \quad t = \hat{t} + \sum_{k=1}^{\infty} c_k(\hat{x}, \hat{t}) \hat{z}^k. \quad (\text{C.3})$$

Plugging into the metric in Poincaré coordinates and comparing with the FG metric order by order, we get:

$$\begin{aligned} b_1 &= c_1 = 0, & a_2 &= b_2 = c_2 = 0, & a_3 &= b_3 = c_3 = 0 & b_4 &= c_4 = 0, \\ a_4 &= -\frac{4A^3 M}{3(A^4 + 2A^2 \hat{t}^2 + 2A^2 \hat{x}^2 + \hat{t}^4 - 2\hat{t}^2 \hat{x}^2 + \hat{x}^4)^{3/2}}. \end{aligned} \quad (\text{C.4})$$

The energy-momentum tensor can be obtained from the results of [59]

$$T_{mn}^{(BH)} = \frac{L}{8\pi G} \lim_{\hat{z} \rightarrow 0} \frac{1}{\hat{z}} \left( K_{mn} - \gamma_{mn} K - \frac{2}{L} \gamma_{mn} \right). \quad (\text{C.5})$$



Here  $\gamma_{mn}$  is the induced metric on a  $\hat{z}$ -constant surface nearby the boundary,  $K_{mn}$  denote the extrinsic curvature tensor calculated with an inward unit vector normal to the  $\hat{z}$ -constant surface, and  $K$  is the trace of the extrinsic curvature tensor.

To explicitly write the components of the energy-momentum tensor, it is convenient to introduce the lightcone coordinates:

$$u^m = (u, v, \phi), \quad u = t - x, \quad v = t + x. \quad (\text{C.6})$$

In these coordinates, the non-vanishing elements of  $T_{mn}^{(BH)}$  are

$$\begin{aligned} T_{uu}^{(BH)} &= \frac{A^3 L^2 M}{8\pi G} \frac{3}{(A^2 + u^2)^{5/2} (A^2 + v^2)^{1/2}}, \\ T_{vv}^{(BH)} &= \frac{A^3 L^2 M}{8\pi G} \frac{3}{(A^2 + v^2)^{5/2} (A^2 + u^2)^{1/2}}, \\ T_{uv}^{(BH)} &= \frac{A^3 L^2 M}{8\pi G} \frac{1}{(A^2 + u^2)^{3/2} (A^2 + v^2)^{3/2}}, \\ T_{\phi\phi}^{(BH)} &= \frac{A^3 L^2 M}{8\pi G} \frac{(u - v)^2}{(A^2 + u^2)^{3/2} (A^2 + v^2)^{3/2}}. \end{aligned} \quad (\text{C.7})$$

## C.2 Monopole with Dirichlet boundary conditions

In order to put the metric with monopole backreaction in FG coordinates, we consider the expansion of  $h$  and  $g$  nearby the boundary in eq. (2.23), setting also  $h_2 = -g_2$ . Then, using the change of variables in eq. (C.3) and solving order by order, we obtain

$$\begin{aligned} b_1 &= c_1 = 0, \quad a_2 = b_2 = c_2 = 0, \quad b_3 = c_3 = 0, \\ a_3 &= \frac{2A^2 g_2}{A^4 + 2A^2 \hat{t}^2 + 2A^2 \hat{x}^2 + \hat{t}^4 - 2\hat{t}^2 \hat{x}^2 + \hat{x}^4}, \\ a_4 &= \frac{4A^3 (g_3 - h_3)}{3(A^4 + 2A^2 \hat{t}^2 + 2A^2 \hat{x}^2 + \hat{t}^4 - 2\hat{t}^2 \hat{x}^2 + \hat{x}^4)^{3/2}}, \\ b_4 &= -\frac{2A^2 g_2 \hat{x} (A^2 - \hat{t}^2 + \hat{x}^2)}{(A^4 + 2A^2 \hat{t}^2 + 2A^2 \hat{x}^2 + \hat{t}^4 - 2\hat{t}^2 \hat{x}^2 + \hat{x}^4)^2}, \\ c_4 &= \frac{2A^2 g_2 \hat{t} (A^2 + \hat{t}^2 - \hat{x}^2)}{(A^4 + 2A^2 \hat{t}^2 + 2A^2 \hat{x}^2 + \hat{t}^4 - 2\hat{t}^2 \hat{x}^2 + \hat{x}^4)^2}. \end{aligned} \quad (\text{C.8})$$

We can now use the generalisation of eq. (C.5) involving scalars [60] to extract the energy-momentum tensor

$$T_{mn}^{(D)} = \frac{L}{8\pi G} \lim_{\hat{z} \rightarrow 0} \frac{1}{\hat{z}} \left( K_{mn} - \gamma_{mn} K - \frac{2}{L} \gamma_{mn} - 4\pi G \frac{\gamma_{mn}}{L} \phi^a \phi^a \right). \quad (\text{C.9})$$

The elements of the energy-momentum tensor in lightcone coordinates look qualitatively similar to the corresponding elements computed in the BH background, see eq. (C.7):

$$\begin{aligned} T_{uu}^{(D)} &= T_{uu}^{(BH)} \left( \frac{16\pi G \alpha_H \beta_H - 3L^2 g_3}{3L^2 M} \right), \\ T_{vv}^{(D)} &= T_{vv}^{(BH)} \left( \frac{16\pi G \alpha_H \beta_H - 3L^2 g_3}{3L^2 M} \right), \\ T_{uv}^{(D)} &= T_{uv}^{(BH)} \left( \frac{-16\pi G \alpha_H \beta_H - 3L^2 g_3}{3L^2 M} \right), \\ T_{\phi\phi}^{(D)} &= T_{\phi\phi}^{(BH)} \left( \frac{32\pi G \alpha_H \beta_H - 3L^2 g_3}{3L^2 M} \right). \end{aligned} \quad (\text{C.10})$$

The Ward identity for  $T_{mn}^{(D)}$  gives

$$\partial^m T_{mn}^{(D)} = \tilde{\beta}_H \partial_n \tilde{\alpha}_H = \langle \mathcal{O}_2 \rangle \partial_n J_D, \quad (\text{C.11})$$

and the trace of the energy-momentum tensor is

$$\eta^{mn} T_{mn}^{(D)} = \tilde{\alpha}_H \tilde{\beta}_H = \langle \mathcal{O}_2 \rangle J_D. \quad (\text{C.12})$$

### C.3 Monopole with Neumann and multitrace boundary conditions

We will follow the approach in [58] to determine the boundary energy-momentum tensor for multitrace deformations. These boundary conditions correspond to adding a finite boundary action  $S_{\mathcal{F}}$  to the renormalised action  $S_{\text{ren}}$

$$S_{\mathcal{F}} = \int d^3x \sqrt{-g_0} (J_F \tilde{\alpha}_H + \mathcal{F}(\tilde{\alpha}_H)), \quad J_{\mathcal{F}} = -\tilde{\beta}_H - \mathcal{F}'(\tilde{\alpha}_H), \quad (\text{C.13})$$

where  $\sqrt{-g_0}$  is the determinant of the boundary metric (at the end of the calculation we will specialise to the Minkowski metric, but it is necessary to keep it in intermediate steps). The variations of the action functionals are:

$$\begin{aligned} \delta S_{\text{ren}} &= \int d^3x \sqrt{-g_0} \left( \frac{1}{2} T^{ij} (\delta g_{(0)})_{ij} + \tilde{\beta}_H \delta \tilde{\alpha}_H \right), \\ \delta S_{\mathcal{F}} &= \int d^3x \sqrt{-g_0} \left( -\tilde{\alpha}_H \delta \tilde{\beta}_H - \tilde{\alpha}_H \mathcal{F}''(\tilde{\alpha}_H) \delta \tilde{\alpha}_H - \tilde{\beta}_H \delta \tilde{\alpha}_H \right), \end{aligned} \quad (\text{C.14})$$

so the total variation is

$$\begin{aligned} \delta S &= \delta S_{\text{ren}} + \delta S_{\mathcal{F}} = \int d^3x \sqrt{-g_0} \left( \frac{1}{2} T^{ij} (\delta g_{(0)})_{ij} - \tilde{\alpha}_H \delta \tilde{\beta}_H - \tilde{\alpha}_H \mathcal{F}''(\tilde{\alpha}_H) \delta \tilde{\alpha}_H \right) \\ &= \int d^3x \sqrt{-g_0} \left( \frac{1}{2} T^{ij} (\delta g_{(0)})_{ij} + \tilde{\alpha}_H \delta J_{\mathcal{F}} \right). \end{aligned} \quad (\text{C.15})$$

Due to the shift of the action, there is also a shift in the energy-momentum tensor:

$$T_{ij}^{(\mathcal{F})} = T_{ij}^{(D)} + \eta_{ij} [\mathcal{F}(\tilde{\alpha}_H) + \tilde{\alpha}_H J_{\mathcal{F}}] = T_{ij}^{(D)} + \eta_{ij} [\mathcal{F}(\tilde{\alpha}_H) - \tilde{\alpha}_H \tilde{\beta}_H - \mathcal{F}'(\tilde{\alpha}_H) \tilde{\alpha}_H]. \quad (\text{C.16})$$

The divergence of the energy-momentum tensor is:

$$\begin{aligned} \partial^i T_{ij}^{(\mathcal{F})} &= \partial^i T_{ij}^{(D)} + \partial_j [\mathcal{F}(\tilde{\alpha}_H) - \tilde{\alpha}_H \tilde{\beta}_H - \mathcal{F}'(\tilde{\alpha}_H) \tilde{\alpha}_H] \\ &= \tilde{\beta}_H \partial_j \tilde{\alpha}_H + \partial_j [\mathcal{F}(\tilde{\alpha}_H) - \tilde{\alpha}_H \tilde{\beta}_H - \mathcal{F}'(\tilde{\alpha}_H) \tilde{\alpha}_H] \\ &= -\tilde{\alpha}_H (\partial_j \tilde{\beta}_H + \mathcal{F}''(\tilde{\alpha}_H) \partial_j \tilde{\alpha}_H), \end{aligned} \quad (\text{C.17})$$

while the trace is:

$$\begin{aligned} \eta^{ij} T_{ij}^{(\mathcal{F})} &= (T^{(D)})^i_i + 3[\mathcal{F}(\tilde{\alpha}_H) - \tilde{\alpha}_H \tilde{\beta}_H - \mathcal{F}'(\tilde{\alpha}_H) \tilde{\alpha}_H] \\ &= -2\tilde{\alpha}_H \tilde{\beta}_H + 3\mathcal{F}(\tilde{\alpha}_H) - 3\tilde{\alpha}_H \mathcal{F}'(\tilde{\alpha}_H). \end{aligned} \quad (\text{C.18})$$

Setting to zero the source  $J_{\mathcal{F}}$  corresponds to

$$\tilde{\beta}_H = -\mathcal{F}'(\tilde{\alpha}_H). \quad (\text{C.19})$$

Note that in this case  $T_{ij}^{(\mathcal{F})}$  is conserved, i.e.  $\partial^i T_{ij}^{(\mathcal{F})} = 0$ .

## D Details of the entanglement entropy calculations

### D.1 Translated-disk region

Defining the polar-like coordinates

$$x_1 = \xi + p \cos \vartheta, \quad x_2 = p \sin \vartheta, \quad (\text{D.1})$$

the entanglement entropy is given by

$$\begin{aligned} \Delta S = & \frac{\pi \alpha_H^2}{2l} \int_0^l dp \frac{p}{(l^2 - p^2)^{3/2}} \int_0^{2\pi} d\vartheta \left[ \frac{(h_\varepsilon + g_\varepsilon) (p^2 \cos^2 \vartheta - l^2) \xi^2 t^2}{\omega_\xi} \right. \\ & + \frac{(h_\varepsilon - g_\varepsilon)}{4} \frac{[p \omega_\xi + 2\xi \cos \vartheta (l^2 - p^2) (l^2 - t^2 + A^2 + \xi^2 + 2\xi p \cos \vartheta)]^2}{\omega_\xi [\omega_\xi + 4A^2 (p^2 - l^2)]} \\ & \left. + \frac{(h_\varepsilon - g_\varepsilon) l^2 \xi^2 \sin^2 \vartheta (l^2 - p^2) (l^2 - t^2 + A^2 + \xi^2 + 2\xi p \cos \vartheta)^2}{\omega_\xi [\omega_\xi + 4A^2 (p^2 - l^2)]} \right], \end{aligned} \quad (\text{D.2})$$

where

$$\omega_\xi \equiv \omega(\sqrt{l^2 + \xi^2 + 2\xi p \cos(2\vartheta)}, t), \quad (\text{D.3})$$

and  $\omega$  is defined in eq. (4.2). In the above integral, both  $h_\varepsilon$  and  $g_\varepsilon$  are functions of

$$r = \frac{1}{2A} \sqrt{\frac{\omega_\xi + 4A^2 (p^2 - l^2)}{l^2 - p^2}}. \quad (\text{D.4})$$

### D.2 Half-plane region

As in eq. (5.10), the  $A$  dependence can be completely reabsorbed introducing the rescaled quantities

$$z \rightarrow \frac{z}{A}, \quad x_2 \rightarrow \frac{x_2}{A}, \quad t \rightarrow \frac{t}{A}. \quad (\text{D.5})$$

Consequently, without loss of generality, from now on we set  $A = 1$ .

For general  $t > 0$ , we can write a closed-form expression for the entropy variation

$$\Delta S = \frac{\pi \alpha_H^2}{8} \int_0^{+\infty} dz \int_{-\infty}^{+\infty} dx_2 \left[ \frac{(h_\varepsilon - g_\varepsilon) (C^2 + 4z^2 x_2^2 D^2)}{z^2 (D^2 + 4t^2)^2} - 4t^2 \frac{(h_\varepsilon + g_\varepsilon) (x_2^2 + z^2)}{z^2 (D^2 + 4t^2)} \right], \quad (\text{D.6})$$

with

$$C \equiv t^4 - z^4 - 2t^2 (x_2^2 - 1) + (x_2^2 + 1)^2, \quad D \equiv -t^2 + x_2^2 + z^2 + 1. \quad (\text{D.7})$$

In the above expression,  $h_\varepsilon(r)$  and  $g_\varepsilon(r)$  are the functions in eq. (2.26), with

$$r = \frac{\sqrt{(-t^2 + x_2^2 + z^2)^2 + 2(t^2 + x_2^2 - z^2) + 1}}{2z}. \quad (\text{D.8})$$

In order to understand the large  $t$  behaviour of the entropy, it is convenient to introduce the variables  $\rho, \gamma$

$$z = \rho \cos \gamma, \quad x_2 = \rho \sin \gamma. \quad (\text{D.9})$$

At large  $t$ , the integrand in eq. (D.6) is non-vanishing just in a region at  $\rho = t \pm \mu$ , with  $\mu$  of order 1. For convenience, we can introduce

$$\rho = t + \delta. \quad (\text{D.10})$$

It turns out that, at large  $t$ , the term proportional to  $(h_\epsilon - g_\epsilon)$  in eq. (D.6) is much smaller than the one proportional to  $(h_\epsilon + g_\epsilon)$ . Moreover, at large  $t$ , we can use the approximation

$$r = \frac{\sqrt{\delta^2 + \sin^2 \gamma}}{\cos \gamma} + O(1/t). \quad (\text{D.11})$$

At the leading order in  $t$ , we find

$$\Delta S = K \alpha_H^2 t, \quad (\text{D.12})$$

where

$$K = -\frac{\pi}{2} \int_0^\infty \frac{r}{1+r^2} \mathbb{E}(-r^2) [h_\epsilon(r) + g_\epsilon(r)] dr. \quad (\text{D.13})$$

$\mathbb{E}$  is the complete elliptic integral, defined as follows

$$\mathbb{E}(m) = \int_0^{\pi/2} d\gamma \sqrt{1 - m \sin^2 \gamma}. \quad (\text{D.14})$$

Numerically, we get the approximate value  $K \approx 0.636$ .

## References

- [1] J. M. Maldacena, “The Large N limit of superconformal field theories and supergravity,” *Adv. Theor. Math. Phys.* **2** (1998) 231–252, [hep-th/9711200](#).
- [2] S. S. Gubser, I. R. Klebanov, and A. M. Polyakov, “Gauge theory correlators from noncritical string theory,” *Phys. Lett. B* **428** (1998) 105–114, [hep-th/9802109](#).
- [3] E. Witten, “Anti-de Sitter space and holography,” *Adv. Theor. Math. Phys.* **2** (1998) 253–291, [hep-th/9802150](#).
- [4] S. Ryu and T. Takayanagi, “Holographic derivation of entanglement entropy from AdS/CFT,” *Phys. Rev. Lett.* **96** (2006) 181602, [hep-th/0603001](#).
- [5] V. E. Hubeny, M. Rangamani, and T. Takayanagi, “A Covariant holographic entanglement entropy proposal,” *JHEP* **07** (2007) 062, [0705.0016](#).
- [6] M. Rangamani and T. Takayanagi, *Holographic Entanglement Entropy*, vol. 931. Springer, 2017. [1609.01287](#).
- [7] J. D. Bekenstein, “Black holes and entropy,” *Phys. Rev. D* **7** (1973) 2333–2346.
- [8] S. W. Hawking, “Particle Creation by Black Holes,” *Commun. Math. Phys.* **43** (1975) 199–220. [Erratum: *Commun.Math.Phys.* 46, 206 (1976)].
- [9] P. Calabrese and J. L. Cardy, “Evolution of entanglement entropy in one-dimensional systems,” *J. Stat. Mech.* **0504** (2005) P04010, [cond-mat/0503393](#).
- [10] J. Abajo-Arrastia, J. Aparicio, and E. Lopez, “Holographic Evolution of Entanglement Entropy,” *JHEP* **11** (2010) 149, [1006.4090](#).
- [11] T. Albash and C. V. Johnson, “Evolution of Holographic Entanglement Entropy after Thermal and Electromagnetic Quenches,” *New J. Phys.* **13** (2011) 045017, [1008.3027](#).
- [12] V. Balasubramanian, A. Bernamonti, J. de Boer, N. Copland, B. Craps, E. Keski-Vakkuri, B. Muller, A. Schafer, M. Shigemori, and W. Staessens, “Thermalization of Strongly Coupled Field Theories,” *Phys. Rev. Lett.* **106** (2011) 191601, [1012.4753](#).

- [13] V. Balasubramanian, A. Bernamonti, J. de Boer, N. Copland, B. Craps, E. Keski-Vakkuri, B. Muller, A. Schafer, M. Shigemori, and W. Staessens, “Holographic Thermalization,” *Phys. Rev. D* **84** (2011) 026010, [1103.2683](#).
- [14] A. Buchel, L. Lehner, and R. C. Myers, “Thermal quenches in  $N=2^*$  plasmas,” *JHEP* **08** (2012) 049, [1206.6785](#).
- [15] A. Buchel, L. Lehner, R. C. Myers, and A. van Niekerk, “Quantum quenches of holographic plasmas,” *JHEP* **05** (2013) 067, [1302.2924](#).
- [16] R. Auzzi, S. Elitzur, S. B. Gudnason, and E. Rabinovici, “On periodically driven AdS/CFT,” *JHEP* **11** (2013) 016, [1308.2132](#).
- [17] A. Buchel, R. C. Myers, and A. van Niekerk, “Nonlocal probes of thermalization in holographic quenches with spectral methods,” *JHEP* **02** (2015) 017, [1410.6201](#). [Erratum: *JHEP* 07, 137 (2015)].
- [18] H. Liu and S. J. Suh, “Entanglement Tsunami: Universal Scaling in Holographic Thermalization,” *Phys. Rev. Lett.* **112** (2014) 011601, [1305.7244](#).
- [19] H. Liu and S. J. Suh, “Entanglement growth during thermalization in holographic systems,” *Phys. Rev. D* **89** (2014), no. 6, 066012, [1311.1200](#).
- [20] H. Casini, H. Liu, and M. Mezei, “Spread of entanglement and causality,” *JHEP* **07** (2016) 077, [1509.05044](#).
- [21] T. Langen, R. Geiger, M. Kuhnert, B. Rauer, and J. Schmiedmayer, “Local emergence of thermal correlations in an isolated quantum many-body system,” *Nature Physics* **9** (2013).
- [22] F. Meinert, M. J. Mark, E. Kirilov, K. Lauber, P. Weinmann, A. J. Daley, and H. Nagerl, “Quantum Quench in an Atomic One-Dimensional Ising Chain,” *Physical Review Letters* **111** (2013).
- [23] I. Klich and L. Levitov, “Quantum Noise as an Entanglement Meter,” *Phys. Rev. Lett.* **102** (2009) 100502, [0804.1377](#).
- [24] J. Cardy, “Measuring Entanglement Using Quantum Quenches,” *Phys. Rev. Lett.* **106** (2011) 150404, [1012.5116](#).
- [25] P. Calabrese and J. Cardy, “Entanglement and correlation functions following a local quench: a conformal field theory approach,” *J. Stat. Mech.* **0710** (2007), no. 10, P10004, [0708.3750](#).
- [26] P. Calabrese and J. Cardy, “Quantum quenches in  $1 + 1$  dimensional conformal field theories,” *J. Stat. Mech.* **1606** (2016), no. 6, 064003, [1603.02889](#).
- [27] M. Nozaki, T. Numasawa, and T. Takayanagi, “Quantum Entanglement of Local Operators in Conformal Field Theories,” *Phys. Rev. Lett.* **112** (2014) 111602, [1401.0539](#).
- [28] P. Caputa, M. Nozaki, and T. Takayanagi, “Entanglement of local operators in large- $N$  conformal field theories,” *PTEP* **2014** (2014) 093B06, [1405.5946](#).
- [29] M. Nozaki, “Notes on Quantum Entanglement of Local Operators,” *JHEP* **10** (2014) 147, [1405.5875](#).

- [30] C. T. Asplund, A. Bernamonti, F. Galli, and T. Hartman, “Holographic Entanglement Entropy from 2d CFT: Heavy States and Local Quenches,” *JHEP* **02** (2015) 171, [1410.1392](#).
- [31] M. Nozaki, T. Numasawa, and T. Takayanagi, “Holographic Local Quenches and Entanglement Density,” *JHEP* **05** (2013) 080, [1302.5703](#).
- [32] C. T. Asplund and A. Bernamonti, “Mutual information after a local quench in conformal field theory,” *Phys. Rev. D* **89** (2014), no. 6, 066015, [1311.4173](#).
- [33] P. Caputa, J. Simón, A. Stikonas, and T. Takayanagi, “Quantum Entanglement of Localized Excited States at Finite Temperature,” *JHEP* **01** (2015) 102, [1410.2287](#).
- [34] M. Rangamani, M. Rozali, and A. Vincart-Emard, “Dynamics of Holographic Entanglement Entropy Following a Local Quench,” *JHEP* **04** (2016) 069, [1512.03478](#).
- [35] J. R. David, S. Khetrapal, and S. P. Kumar, “Universal corrections to entanglement entropy of local quantum quenches,” *JHEP* **08** (2016) 127, [1605.05987](#).
- [36] C. A. Agón, S. F. Lokhande, and J. F. Pedraza, “Local quenches, bulk entanglement entropy and a unitary Page curve,” *JHEP* **08** (2020) 152, [2004.15010](#).
- [37] T. Shimaji, T. Takayanagi, and Z. Wei, “Holographic Quantum Circuits from Splitting/Joining Local Quenches,” *JHEP* **03** (2019) 165, [1812.01176](#).
- [38] A. Jahn and T. Takayanagi, “Holographic entanglement entropy of local quenches in AdS<sub>4</sub>/CFT<sub>3</sub>: a finite-element approach,” *J. Phys. A* **51** (2018), no. 1, 015401, [1705.04705](#).
- [39] D. S. Ageev, “Sharp disentanglement in holographic charged local quench,” [2003.02918](#).
- [40] G. ’t Hooft, “Magnetic Monopoles in Unified Gauge Theories,” *Nucl. Phys. B* **79** (1974) 276–284.
- [41] A. R. Lugo and F. A. Schaposnik, “Monopole and dyon solutions in AdS space,” *Phys. Lett. B* **467** (1999) 43–53, [hep-th/9909226](#).
- [42] A. R. Lugo, E. F. Moreno, and F. A. Schaposnik, “Monopole solutions in AdS space,” *Phys. Lett. B* **473** (2000) 35–42, [hep-th/9911209](#).
- [43] S. Bolognesi and D. Tong, “Monopoles and Holography,” *JHEP* **01** (2011) 153, [1010.4178](#).
- [44] P. Sutcliffe, “Monopoles in AdS,” *JHEP* **08** (2011) 032, [1104.1888](#).
- [45] S. Bolognesi, J. N. Laia, D. Tong, and K. Wong, “A Gapless Hard Wall: Magnetic Catalysis in Bulk and Boundary,” *JHEP* **07** (2012) 162, [1204.6029](#).
- [46] S. Prem Kumar, A. O’Bannon, A. Pribytok, and R. Rodgers, “Holographic Coulomb branch solitons, quasinormal modes, and black holes,” *JHEP* **05** (2021) 109, [2011.13859](#).
- [47] A. R. Lugo, E. F. Moreno, and F. A. Schaposnik, “Holographic Phase Transition from Dyons in an AdS Black Hole Background,” *JHEP* **03** (2010) 013, [1001.3378](#).
- [48] A. R. Lugo, E. F. Moreno, and F. A. Schaposnik, “Holography and AdS<sub>4</sub> self-gravitating dyons,” *JHEP* **11** (2010) 081, [1007.1482](#).

- [49] G. L. Giordano and A. R. Lugo, “Holographic phase transitions from higgsed, non abelian charged black holes,” *JHEP* **07** (2015) 172, [1501.04033](#).
- [50] S. Miyashita and K.-i. Maeda, “AdS Monopole Black Hole and Phase Transition,” *Phys. Rev. D* **94** (2016), no. 12, 124037, [1610.07350](#).
- [51] A. Esposito, S. Garcia-Saenz, A. Nicolis, and R. Penco, “Conformal solids and holography,” *JHEP* **12** (2017) 113, [1708.09391](#).
- [52] G. T. Horowitz and N. Itzhaki, “Black holes, shock waves, and causality in the AdS / CFT correspondence,” *JHEP* **02** (1999) 010, [hep-th/9901012](#).
- [53] T. Albash and C. V. Johnson, “Holographic Studies of Entanglement Entropy in Superconductors,” *JHEP* **05** (2012) 079, [1202.2605](#).
- [54] E. Witten, “Multitrace operators, boundary conditions, and AdS / CFT correspondence,” [hep-th/0112258](#).
- [55] M. Berkooz, A. Sever, and A. Shomer, “‘Double trace’ deformations, boundary conditions and space-time singularities,” *JHEP* **05** (2002) 034, [hep-th/0112264](#).
- [56] I. Papadimitriou, “Multi-Trace Deformations in AdS/CFT: Exploring the Vacuum Structure of the Deformed CFT,” *JHEP* **05** (2007) 075, [hep-th/0703152](#).
- [57] T. Faulkner, G. T. Horowitz, and M. M. Roberts, “Holographic quantum criticality from multi-trace deformations,” *JHEP* **04** (2011) 051, [1008.1581](#).
- [58] M. M. Caldarelli, A. Christodoulou, I. Papadimitriou, and K. Skenderis, “Phases of planar AdS black holes with axionic charge,” *JHEP* **04** (2017) 001, [1612.07214](#).
- [59] V. Balasubramanian and P. Kraus, “A Stress tensor for Anti-de Sitter gravity,” *Commun. Math. Phys.* **208** (1999) 413–428, [hep-th/9902121](#).
- [60] S. de Haro, S. N. Solodukhin, and K. Skenderis, “Holographic reconstruction of space-time and renormalization in the AdS / CFT correspondence,” *Commun. Math. Phys.* **217** (2001) 595–622, [hep-th/0002230](#).
- [61] S. A. Hartnoll, C. P. Herzog, and G. T. Horowitz, “Building a Holographic Superconductor,” *Phys. Rev. Lett.* **101** (2008) 031601, [0803.3295](#).
- [62] J. Bhattacharya, M. Nozaki, T. Takayanagi, and T. Ugajin, “Thermodynamical Property of Entanglement Entropy for Excited States,” *Phys. Rev. Lett.* **110** (2013), no. 9, 091602, [1212.1164](#).
- [63] D. D. Blanco, H. Casini, L.-Y. Hung, and R. C. Myers, “Relative Entropy and Holography,” *JHEP* **08** (2013) 060, [1305.3182](#).
- [64] A. O’Bannon, J. Probst, R. Rodgers, and C. F. Uhlemann, “First law of entanglement rates from holography,” *Phys. Rev. D* **96** (2017), no. 6, 066028, [1612.07769](#).
- [65] H. Casini, M. Huerta, and R. C. Myers, “Towards a derivation of holographic entanglement entropy,” *JHEP* **05** (2011) 036, [1102.0440](#).
- [66] T. Albash and C. V. Johnson, “Vortex and Droplet Engineering in Holographic Superconductors,” *Phys. Rev. D* **80** (2009) 126009, [0906.1795](#).
- [67] M. Montull, A. Pomarol, and P. J. Silva, “The Holographic Superconductor Vortex,” *Phys. Rev. Lett.* **103** (2009) 091601, [0906.2396](#).



- [68] V. Keranen, E. Keski-Vakkuri, S. Nowling, and K. P. Yogendran, “Inhomogeneous Structures in Holographic Superfluids: II. Vortices,” *Phys. Rev. D* **81** (2010) 126012, [0912.4280](#).
- [69] O. Domenech, M. Montull, A. Pomarol, A. Salvio, and P. J. Silva, “Emergent Gauge Fields in Holographic Superconductors,” *JHEP* **08** (2010) 033, [1005.1776](#).
- [70] N. Iqbal and H. Liu, “Luttinger’s Theorem, Superfluid Vortices, and Holography,” *Class. Quant. Grav.* **29** (2012) 194004, [1112.3671](#).
- [71] O. J. C. Dias, G. T. Horowitz, N. Iqbal, and J. E. Santos, “Vortices in holographic superfluids and superconductors as conformal defects,” *JHEP* **04** (2014) 096, [1311.3673](#).
- [72] K. Maeda, M. Natsuume, and T. Okamura, “Vortex lattice for a holographic superconductor,” *Phys. Rev. D* **81** (2010) 026002, [0910.4475](#).
- [73] G. Tallarita, R. Auzzi, and A. Peterson, “The holographic non-abelian vortex,” *JHEP* **03** (2019) 114, [1901.05814](#).
- [74] G. Tallarita and R. Auzzi, “The holographic vortex lattice using the circular cell method,” *JHEP* **01** (2020) 056, [1909.05932](#).
- [75] L. Susskind, “Computational Complexity and Black Hole Horizons,” *Fortsch. Phys.* **64** (2016) 24–43, [1403.5695](#). [Addendum: *Fortsch.Phys.* 64, 44–48 (2016)].
- [76] D. Stanford and L. Susskind, “Complexity and Shock Wave Geometries,” *Phys. Rev. D* **90** (2014), no. 12, 126007, [1406.2678](#).
- [77] A. R. Brown, D. A. Roberts, L. Susskind, B. Swingle, and Y. Zhao, “Holographic Complexity Equals Bulk Action?,” *Phys. Rev. Lett.* **116** (2016), no. 19, 191301, [1509.07876](#).
- [78] M. Moosa, “Evolution of Complexity Following a Global Quench,” *JHEP* **03** (2018) 031, [1711.02668](#).
- [79] S. Chapman, H. Marrochio, and R. C. Myers, “Holographic complexity in Vaidya spacetimes. Part I,” *JHEP* **06** (2018) 046, [1804.07410](#).
- [80] S. Chapman, H. Marrochio, and R. C. Myers, “Holographic complexity in Vaidya spacetimes. Part II,” *JHEP* **06** (2018) 114, [1805.07262](#).
- [81] B. Chen, W.-M. Li, R.-Q. Yang, C.-Y. Zhang, and S.-J. Zhang, “Holographic subregion complexity under a thermal quench,” *JHEP* **07** (2018) 034, [1803.06680](#).
- [82] R. Auzzi, G. Nardelli, F. I. Schaposnik Massolo, G. Tallarita, and N. Zenoni, “On volume subregion complexity in Vaidya spacetime,” *JHEP* **11** (2019) 098, [1908.10832](#).
- [83] G. Di Giulio and E. Tonni, “Subsystem complexity after a global quantum quench,” *JHEP* **05** (2021) 022, [2102.02764](#).
- [84] D. S. Ageev, I. Y. Aref’eva, A. A. Bagrov, and M. I. Katsnelson, “Holographic local quench and effective complexity,” *JHEP* **08** (2018) 071, [1803.11162](#).
- [85] D. Ageev, “Holographic complexity of local quench at finite temperature,” *Phys. Rev. D* **100** (2019), no. 12, 126005, [1902.03632](#).
- [86] G. Di Giulio and E. Tonni, “Subsystem complexity after a local quantum quench,” [2106.08282](#).